Master's thesis

NTNU
Norwegian University of Science and Technology
Faculty of Natural Sciences
Department of Materials Science and Engineering

Sondre Bolstad Bjørø

Interface studies on BT-coatings on Ti-alloys using Atom Probe Tomography

Master's thesis in Structural Chemistry
Supervisor: Assoc. Prof. Julia Glaum
Co-supervisor: Dr. Magnus Rotan
July 2021

NTNU
Norwegian University of
Science and Technology

Sondre Bolstad Bjørø

Interface studies on BT-coatings on Ti-alloys using Atom Probe Tomography

Master's thesis in Structural Chemistry
Supervisor: Assoc. Prof. Julia Glaum
Co-supervisor: Dr. Magnus Rotan
July 2021

Norwegian University of Science and Technology
Faculty of Natural Sciences
Department of Materials Science and Engineering

NTNU
Norwegian University of
Science and Technology

Abstract

This master thesis aims to study the interface of laser textured Ti6Al4V substrates spin coated with a $BaTiO_3$ piezoelectric coating, using Atom Probe Tomography. The coated samples was previously produced by Marcus Solum for the purpose of developing a piezo-electric coating for orthopedic implants. This thesis will be a continuation of his work where the interface will be studied as Solum was not able to do that successfully in his work. The primary motivation for this continuation is to evaluate if the use of atom probe tomography is a valid approach for interface analysis for these materials and determine what information is possible to obtain from these analyses.

The main focus of the thesis is put on the analysis and sample preparation method and the considerations that needs to be made when these are applied to sub optimal and fragile samples. The working principles and theory behind atom probe as an analysis method are described and discussed with the aim of giving an understandable and sufficient insight to the method to be able to make apply the method to a similar material system, with equal challenges with little to none prior experience.

The material samples prepared by Solum proved to be highly porous around the interface. This resulted in fragile atom probe samples which proved challenging to prepare, analyse and reconstruct. Out of the 36 samples prepared only 4 was successfully analysed where one of them can be considered to provide a complete picture of the evolution in composition across the interface. The $BaTO_3$ coating layer was not conclusively found in the analysis.

By analysis of the interface it was determined that the nitrogen introduced in the production of the sample has accumulated close to the Ti6Al4V substrate in the form of TiN the remaining interface region primarily consist of TiO_2 that rapidly decreased in concentration towards the Ti6Al4V substrate. The vanadium has diffused from the substrate throughout the entire interface region and accumulated as a separate phase in the upper part of the interface region.

Different measures to reduce sample failure and overcome the challenges that arises from the high porosity in the samples have been explored and discussed, among these are experimentation with different protection layers, deposition soldering and adjustments in the analysis parameters.

Sammendrag

Denne Master oppgaven tar for seg interfase studier av interfasen mellom laser teksturete Ti6Al4V substrat og piezoelektriske tynnfilmer ved bruk av atom probe tomografi. Materialprøvene som blir brukt i denne oppgaven ble produsert av Markus Solum som en del av hans master prosjekt i 2020. hovedmotivasjonen for å bruke disse prøvene er å evaluere hvorhvidt atom probe er en gunstig analysemetode for denne typen prøver, som ikke er laget med tanke på atom probe, samt å evaluere hvilken informasjon som er mulig å hente fra disse analysene.

Hovedfokuset i oppgaven ligger på analysemetoden og prøveprepareringen og hvliken hensyn som må tas når denne prossesen anvendes på relativt skjøre prøver, som ikke i utgangspunktet er ergnet for analyse med atom probe. Hovedtrekkende og prinsippene rundt analysemetoden og prøverprepareringen er beskrevet og diskuter med et mål om at det skal være mulig å anvende eller å adoptere metoden til lignende materialer og utfordringer uten særskilt stor erfaring fra atom probe analyser fra før.

Prøvene produsert av markus solum iste seg å være rimelig porøse, og realtivt dårlig egnet til analyse med atom probe. Dette førte til utfordringer under analyse og forberedelse av prøvene. Av 36 forberedte prøver ble bare 4 av analysene vellyket, hvorav en av de ga et så komplett datasett at den kan ansees å gi en komplett beskrivelse av komposisjonsutviklingen i interfase regionen.

ved analyse av denne prøven ble det funnet at Nitrogenet som ble introdusert som en del av produksjonprosessen har ansamlet seg nærme metall-substarte i form av titan nitrid. Resten av interfase regionen ble funnet å hovedakelig bestå av titandioksid med en synkende konstresjon mot metallsubstratet. Vanadium fra substratet ble også funnet å diffusere uhindretgjennom hele interfase regionen og danne en egen fase i det øvre sjiktet av interfase regionen.

Ulike tiltak for å hindre brudd i prøvene ble utforsket og diskutert, blandt annet utprøving av ulike besyttelsesfilmer, forsterking av porøse områder med deposisjon og justeringer av analyseparameterene.

Acknowledgements

I express my sincerest gratitude towards my supervisor Assoc. Prof. Julia Glaum and my co-supervisor Dr. Magnus Rotan for their encouragements and guidance in this work for this thesis. They have showed me both patience, understanding and resourcefulness that has been invaluable in every challenges i have faced during my work the past year. My thanks also continues to the rest of the FACET group which have provided a great enviorment for learning and exchange of experience through our weekly meetings.

i would also like to thank senior engineer Constantinos Hatzoglou for his guidance and assistance in the atom probe analyses and his patience through the many failed attempts. He also deserves my praise for his great work in developing and sharing of the data treatment software NAPA. I would also like to thank PhD. candidate Kasper Aas Hunnestad, he has been my mentor and guide through sample preparation and have readily shared his ideas with me and helped whenever i needed and for that I'm truly grateful.

i would also like to thank all the great staff of NORFAB NanoLab, as well as acknowledge the NORFAB organisation for the use of their state of the art laboratory facility.

Contents

List of Figures

List of Tables

1 Introduction

In this master thesis the interfaces of previously made samples of $BaTiO_3$ (BT) coatings on textured laser textured Ti6Al4V substrates were to be analysed using atom probe tomography (APT). The samples were made for use in biomedical applications, to explore the possibilities of coating pre-textured substrates with a piezoelectric ceramic coating. A piezoelectric coating is believed to enhance the integration of orthopedic implants in the body, as it more closely mimic the behaviour of natural bone and stimulate tissue growth around the implant[6]. The samples was made by Marcus Solum as a part of his master thesis in 2020[16]. In his project the interface of the samples was not successfully characterised as he could not achieve sufficient resolution using EDS scans. There were several initial questions about the interface raised. A substantial TiO_2 layer was observed between the metallic substrate and the BT. The composition and evolution of this layer was of great interest as it influences the adhesion and performance of the coating. The samples were also laser textured, the influence of this texturing might have on the coating and on the interface is also highly interesting as this is a major aspect of the prepared samples. Marcus Solum also reported an unknown secondary phase, in on one of the substrates with the highest degree of laser surface modifications. this secondary phase was hypothesised to be the result of an interface interaction and was therefore of high interest to investigate.

The main goal of this master thesis is to determine if APT is a suitable characterisation method for the textured BT samples. The quality of the sample is of major importance for a successful APT analysis. And has a major influence on the quality of the data obtained or if the analysis is at all possible to perform. The existing literature of APT analyses does not contain any published studies done on BT. The existing literature is also highly focused around high quality samples,specially produced for APT. Exploratory and experimental samples are rarely given considerations for APT analysis as pores, poor adhesion and uncertain compositions are factors that reduces the quality of the data obtainable and makes an APT analysis difficult. One or more of these factors are often present in exploratory produced samples and if samples like this can be analysed by APT, even with a decreased data quality. A powerful tool for material development and characterisation is made available.

Another motivation for this project is that NTNU recently acquired a modern atom probe of the type Cameca LEAP 5000 XS. The expertise and knowledge in operation of this instrument is rapidly growing at NTNU but the use is largely limited to a small group of users. The large amount of unused capacity of the instrument gives research groups at NTNU a unique possibility to try out and possibly adopt APT as a characterisation method for a broad range of samples not initially intended for APT. This thesis will therefore try to highlight the challenges and possibilities to overcome them, when trying to analyse a low quality yet complex sample. An emphasis will also be given to what considerations needs to be made when evaluating if a sample is suitable for APT analysis, and what kind of data one can expect to obtain from them.

The secondary goal of the thesis is to achieve a series of successful analyses and study the composition and evolution of the BT thin film. Pinpoint features introduced by the sample preparation method and identify the influence the laser texturing have had on the composition of the films. the main focus will be on the interface region which is the region that Marcus Solum previously has been unable to characterise.

2 Background

2.1 Principles of Atom Probe Tomography

2.1.1 working principles of APT

Atom probe tomography (APT) is a method used for imaging the chemical composition of solid materials. APT gives a spatial resolution close to atomic level and a compositional sensitivity of 10 ppm. The working principles behind the APT is relatively simple in theory. The needle shaped sample is ionized and evaporated by an electric field in vacuum. To achieve a controlled and sequential evaporation of the sample, an energy source in the form of a laser or variations in the electric field is pulsed towards the tip of the sample in short pulses, inducing the evaporation of the sample at a known time. The ions leaving the sample is then led by the electric field towards a detector and the mass over charge ratio is measured by the time of flight[14].Figure 2.1 despict a simplified illustration on the core working principles and instrument design of APT.

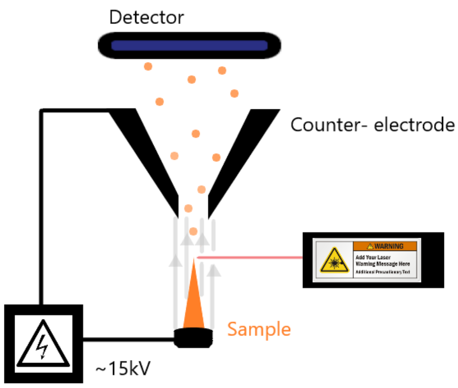

Figure 2.1: Simplified illustration of the core design of an atom probe. A needle shaped sample is positioned close to a local electrode, subjected to a high electric field and pulsed by a laser. the sample starts to emit ions due to the field evaporation mechanisms described in **??** and the emitted ions are detected by a detector.

Despite its simple working principles of the analysis, it does in practice require a very fine mechanical and technical instrumentation, such as position-sensitive detectors, a precise laser beam, cryogenic chamber etc.., which makes the instrumentation expensive to build and maintain. The samples that can be analyzed are also limited primarily in size. The tip of the needles needs to be below 100 nm thick in in order to be ionized with a reasonable electric field which severely limits the width of the sample. As the tip is continuously evaporated the tip of the needle is also flattened, this limits the depth of the sample to below 1 µm, as the required electric field will progressively become higher until It is no longer possible to evaporate the tip of the sample in a controlled manner.

The use of APT was initially reserved for metals as they show conducting properties and was compatible with the high voltage pulsing which was the first method of energy pulsing used. With the advent of laser induced evaporation a wide range of materials such as semiconductors, dielectrics and even biological materials can be analyzed, however with a slightly lower resolution compared to metals.

2.1.2 principles of field evaporation

In APT a very sharp needle is subjected to an electric potential which is typically in the range of 2-10 kV. When the sample is subjected to an external electric field, the electrons of the material is displaced slightly inwards towards the bulk of the sample. Leaving partially positively charged atoms on the surface of the sample. When this polarization of the material is sufficiently strong, one of the atoms may be pulled completely away from the bulk of the sample, leaving the electron behind and leave the sample as an ion. The field strength required to achieve this is called the field of zero barrier evaporation. The evaporated ion is then accelerated by the electric field and can be detected at a detection screen. The field of zero evaporation barrier is material dependant and is determined by the ionization energy and the evaporation energy of the material in question. The principles behind this polarization is quite complex and not fully understood, so it will only be described in it most basic terms here[14**?**].

In order to achieve a very strong electric field to match the field of zero barrier evaporation. The samples in APT is shaped like needles with an tip radius of around . The sharp tip allows for a strong induced field towards the apex of the tip under a reasonable applied field. In order to estimate the induced field (F) at the apex of the needle it is assumed that the needle has the shape of a half sphere with a radius of curvature (R). however, since the needle is not completely hemispherical, the shank of the tip creates a deviation from a spherical geometry. To account for this a field intensity factor (kf) is defined and added as a term in the ideal expression for electrostatic potential over a half-sphere, which gives the approximation for the induced field (F)[8]:

$$F = \frac{V}{k_f R}$$

Where V is the applied external field. When this induced field is strong enough to match the field of zero evaportion barrier. Field evaportion can be facilitated and the analyisis can be conducted.

The field intensity factor (kf) or field factor as it is commonly referred to typically have a value between 3 and 8. The field factor changes based on the properties of the sample, where geometry is the primary contribution. A very sharp tip will have a small shank angle,i.e the angle or rate of which the needle apex tapers off is very fast. This will lead to a stronger intensification towards the tip and subsequently a lower field factor. As the tip of the needle is continuously evaporated, the tip will progressively become wider. As this happens the induced field required for evaporation will increase, which will be noticed by an increase in the applied field before evaporation occurs. It is however assumed that the shape of the needle will remain constant and not change during the analysis, as the sample will assume an equilibrium geometry that minimizes the total surface energy. [8]

A correct field factor is crucial for the result of the analysis since it is an influential parameter for the reconstruction of the tomogram. The field factor is usually determined by either a profiling of the tip or by estimation based on an initial known tip radius of the sample and the evolution of the voltage curve during the analysis. However unpredictable features of the sample may skew these estimations. The effects of low energy facet creations may create a magnitude of very sharp, local tips, which will falsely reduce the observed field factor. Cavities and pores in the sample may similarly split the apex of the needle creating a similar effect[8].

2.2 Practical aspects of APT analysis

An ATP analysis is simply conducted by applying an electric field that is amplified at the apex of a very thin sample. The sample is subjected to a field with a strength that is barely not enough to spontaneously evaporate the apex of the sample. In laser assisted evaporation, a precise laser is focused at the very peak of the sample. The energy of the laser can be manipulated and it is used to rapidly pulse the sample with short pulses with a pulse duration around 200 fs. The aim is to introduce energy to the sample and induce a field evaporation at precise and known points in time. Evaporation events that occurs in the sample as a result of the pulsing is assumed to happen instantly and by knowing the timing of the evaporation event, the evaporated ions can be detected by a position sensitive amplifying detector and the time of flight can be calculated. when the time of flight is known the mass to charge ratio of the detected ion can be determined, which identifies the evaporated ion. This rapid switching between energy levels that can facilitate evaporation and a level where evaporation events are unlikely, can as well be achieved by rapidly fluctuating the applied field. This is called a high voltage pulsing (HV-pulsing) and is only effective for samples with conductive properties. As non conductive samples can not respond to the changes in field strength fast enough to achieve a precise timing of the evaporation events. Non conductive samples are therefore restricted to the use of the laser assisted evaporation. Because the samples relevant for this project does not have conductive properties, the primary focus will be on laser assisted evaporation going forward in this project.

The energy and of the pulsed laser is an important analysis condition and the appropriate pulse energy is largely tied to the evaporation properties of the material to be analysed. A too high pulse energy introduces an excessive amount of energy to the sample and this may have negative influences on the quality of the data obtained. If the amount of energy introduced are so large that it can not be rapidly dissipated after the pulse, the sample may continue to emit long after the pulse is finished. This increases the time window when evaporation events are likely to occur. the longer the sample is able to evaporate after the pulse the larger the uncertainty in the timing of the evaporation becomes, as it is assumed that the evaporation occurs in an instant at the start of the pulse. this same effect can occur in samples with a low thermal conductivity, the sample is locally heated by the laser and unable to dissipate the heat at a sufficient rate. For this reason samples with a low thermal conductivity is more sensitive to increases in pulse energy. An excessive pulse energy also increases the number of higher charged ions and ionic clusters detected from the sample. cluttering the mass spectra and increases the chance of overlaps in the spectra as well as reducing the efficiency of the analysis.[8, 14]

A too low pulse energy is problematic as it can lead to a preferential evaporation of certain species in the sample. Preferential evaporation happens when some elements or phases of the sample have a large discrepancy in field of evaporation compared to one another, resulting in some components of the sample are evaporate far easier than other components. The easy to evaporate components may be evaporated by an energy which is insufficient to evaporate the the hard to evaporate components. resulting, in a drastic misrepresentation of the composition of the sample. To limit the impact of preferential evaporation, the pulse energy can be increased to a level where all the components are evaporated. However by doing this, the easier to evaporate components of the sample will start to experience the negative effects of an excessive pulse energy described earlier. Specific for laser assisted evaporation there is also possible to experience a geometric preferential evaporation, where some area of the sample is more likely to be evaporated before other[**?**] This effect is most apparent at high pulse energies and for materials with a low heat conductivity. This phenomena is a result of the laser being pulsed from one side of the sample and the part of the sample facing the laser experience a higher pulsing energy compared to the side that is facing away from the laser.

The pulse frequency also has an influence on the analysis. The effect of the pulse frequency is however easier to predict and have a broader range of suitable configurations. The pulse frequency describes how often the sample is pulsed. This is varied based on the type of material to be analysed, large clusters or heavy ions requires a longer time to reach the detector compared to lighter ones. For analysis of these heavier ions, this extra time needs to e taken into account by reducing the pulse frequency. If the pulse frequency is set to low the lighter ions of subsequent pulse may catch up with the heavy ions of the last pulse. This creates artefacts in the mass spectrum, as ions hitting the detector in the relevant time window are assumed to be a result of the corresponding pulse[8]. There is no significant downside of having a slightly to low pulse frequency other than the cycle time of each pulse is increased and the analysis time is increased as a result of this.

The base temperature of the analysis is also performed at cryogenic temperatures, often as low as 20 K. This is done to limit the possibilities of surface diffusion under the analysis. The lower the temperature the lower is the possibilities for surface diffusion to occur and the higher the quality of the analysis is. a lower temperature also help to reduce the mobility of any residual gas molecules that might have adsorbed to the sample and its arrangement. This improves the vacuum of the analysis chamber and subsequently reduce the background levels in the analysis[9]. The downside of reducing the temperature of the analysis is that it may make the sample more brittle and more susceptible to fracturing early. Depending on the quality of the sample a compromise must therefore be between quality of the analysis and the sample yield when determining the analysis base temperature[14].

The final parameter significant for the analysis is the detection rate (DR) the detection rate is given in % and dictates how fast the tip is desired to be evaporated. APT experiments are usually set up to keep a fixed detection rate throughout the analysis. To achieve this the applied voltage applied is varied to regulate the detection rate. As the sample evolves and the tip becomes more blunt the required potential to keep the detection rate constant increases. The higher the detection rate the higher this voltage will be and therefore will a increase in detection rate increase the possibilities for a premature sample fracture. The Signal to noise ratio does however increase with an increased detection rate. The detection rate is therefore typically set as high as possible Sometimes up to 5 % for easy to evaporate samples, while still maintaining an acceptable yield[14, 8]

2.2.1 Reconstruction

After the analysis data is obtained the volume of the sample needs to be reconstructed in order to be analysed. The theories and algorithms behind reconstructions are very complex and outside the scope of this project, the basic principles and practical considerations will however be explained in the following section.To reconstruct the volume of the sample one need to calculate the point of origin for each of the ions hitting the detector based on the detected position. To do this one need to calculate the distance between the sample and the detector, the field the ion was experiencing at the time of evaporation and the geometry of the sample in order to accurately estimate its trajectory.

During reconstruction the sample is assumed to have a symmetrical, hemispherical tip with a tip radius R this tip radius can be calculated at all point during the analysis through the field factor of the sample and the evaporation properties of the material by utilizing the relation[8]:

$$R = \frac{V}{k_f F_e}$$

Where V is the applied voltage, kf is the field factor and Fe is the field of evaporation for the given material Fe is assumed to be constant for a given volume of the sample. This way the continuous evolution of the tip can be estimated through the entire analysis by the variation of the applied field.

The field factor is an important as this describes the shape of the tip and are assumed to remain constant throughout the analysis. This value is also utilized to describe the field landscape around the tip and subsequently the acceleration of the evaporated ions. this field factor can be estimated by several different methods. The simplest is to profile an SEM image of the sample and determine a field factor based on the visual geometry of the sample. This might however give a wrong value as the prepared sample tip might not be in it equilibrium lowest surface energy state, and the shape might be altered once the analysis starts. To makes this more reliable the field factor can be compared and adjusted based on angle of the sample, which is possible to determine based on how fast the tip radius is increased over a set distance.[8]

The experienced field at the apex of the tip (F) can be described by the electrostatic potential over a curved surface with a radius (R), corrected for deviation in a spherical geometry by the field factor (kf):

$$F = \frac{V}{k_f R}$$

This approximation gives the experienced field at the surface of the sample it does however not describe the field in the close vicinity to the tip. This field landscape surrounding the sample is complex and requires comprehensive simulations to model. Models like this have been made and the field landscape surrounding in the tip is possible to correlate to the field factor and radius of the tip[8]

The mean distance between the apex of the tip is the last parameter needed to be obtained in order to accuratly project the trajectories of the detected ions. This is done by using one or more of the obtained group of ions and defining their mass to the known mass of that particular ion in the reconstruction protocol. By doing this the distance can be continuously calibrated by calculating the distance travelled by these ions based on their time of flight. as opposed to using their time of flight to determine their mass, as this is alredy predefined [**?**]

2.2.2 Sample requirements

The quality of the sample directly influences the quality of the analysed data. The quality of the sample is also large factor that influences the probability of a premature fracture in the sample. The first requirement is that sample needs to have a smooth surface without protrusions or grooves.The tip also needs to be hemispherical, with a circular cross section and a Radius of curvature of 50-150 nm. This is important for two primary reasons. Firstly the the reconstruction algorithms used for reconstruction of the obtained data assumes a hemispherical tip. Deviations from this geometry will alter and skew the results during the reconstructions, reduce the spacial resolution as well as misrepresenting the true geometry of the sample. The other primary aspect of this requirement, is that small protrusions or grooves are areas that can facilitate field evaporation. This may result in evaporation from other areas than the tip and skews the TOF measurements as these are evaporated further from the detector compared to the main tip. Protrusions and grooves also disturb the way the apex of the tip evolves during the analysis, making the evolution unpredictable. This invalidates the estimated field factor,resulting in a wrong description the sample geometry and further distorts the reconstruction[14].

The tip does as well need to be free of secondary peaks, peaks which are not the primary peak, but sharp residual parts of the surrounding post or sample, closer than 10 um to the primary peak. Secondary peaks leads to evaporation events that is not associated to the sample itself and may lead to an increased background signal in the analysis or false signals in the mass spectra. Where the evaporation from the secondary peaks are detected in the same time frame as a valid evaporation event from the primary peak.[8]

The placement of the region of interest should not be directly at the apex of the tip, but typically 100 nm bellow [**?** 7]. Under the initial parts of the analysis some of analysed sample volume is expected to be discarded. In the initial stage of the analysis the tip of the sample is undergoing changes before it reaches its equilibrium state. Prepared samples are rarely perfectly hemispherical and the apex of the sample therefore needs to adjust to its hemispherical equilibrium. Are not evaporated under the assumed conditions for the analysis and can therefore not be accurately reconstructed after the analysis. How much of the sample volume lost in this initial phase of the analysis is greatly influenced by the initial sample geometry and the overall width of the sample. The time it takes to focus and adjust the laser under laser assisted evaporation also leads to a loss of volume in this initial stage of the sample analysis.

The final sample requirement needed to be considered is the shank angle. The shank angle is described as the angle of the tip in relation to a vertical cylinder and describes how fast the sample tapers as shown in fig 2.2. The shank angle influence how fast the radius of the tip increases during the analysis and subsequently how fast the tip becomes too blunt to facilitate the field evaporation. This influences the expected depth of the sample possible to analyse and for this reason it needs to be small[12]. There are however other considerations to be taken , for laser assisted evaporation the increased area that becomes available with a larger shank angle and the subsequent increase in tip radius. Are observed to increase the mass resolution as the larger area facilitates a more rapid dissipation of energy, quickly allowing the apex of the sample to dissipate its thermal energy and bring it back under the evaporation threshold faster. This shortens the time window for which evaporation can occur and subsequently increase the mass resolution.[8]

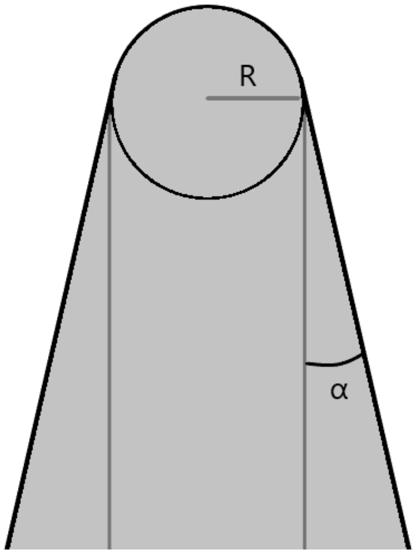

Figure 2.2: visual representation of the shank angle, $\alpha, and the tip radius, R$

2.2.3 Previus work on similar material systems

In recent years the innovations in laser technology have made the laser pulse assisted evaporation in atom probe both reliable and fast. This has greatly widened the applications for APT as it can now be used for non conductive samples, such as oxides and semiconductors. In the earlier generations of atom probes the only reliable way to pulse the sample was using a high voltage pulse which is only possible if the material is conductive. Several different material systems has already been reported analysed, however there was not found any specific studies previously done on $BaTiO_3$. This is unfortunate as the optimal analysis parameters are very material dependent. Because the mechanisms governing the field evaporation and how the different material properties influence the analysis is difficult to predict. This is especially true for complex material systems with interactions from several different elements or phases which is the case for the $BaTiO_3$ coated samples. Thin films poses yet again a challenge in several material systems as the field of evaporation is expected to potentially change quickly, disturbing the propagation of the sample tip and creating artefacts during reconstruction [19].

One reported analysis of a similar material system was done on a PZT ($Pb(Zr_Ti)O_3$) thin film. This is a similar piezoelectric oxide material with a perovskite structure with a similar composition to BaTiO. The samples was specifically made for APT analysis with and depostited on a SiO_2 substrate with a Pt adhesion layer in between.[12] these samples where reported analysed at 50K with a pulse energy between in the range of 0,2 -2,2 pJ. Despite being able to produce samples with no porosity and good adhesion between the PZT and the substrate layer, it was still reported frequent fractures and difficulties in obtaining high quality reconstructions due to evaporation abnormalities during the analysis. For sample preparation it was suggested a shank angle of around 5 °and Tip radius between 50 and 100 nm.

In APT, the sample quality is important in order to achieve a good and valid result. There was not found any reported results for low quality samples with large amounts of porosity that can be comparable to the samples in this project. For APT analysis it is common to prepare samples specifically for the purpose by carefully eliminating pores and compositions with a vastly different evaporation energy, especially when studying new material systems. There is however examples of alterations to the sample preparation technique where the condition of an initial porous and low quality sample was completely encapsulated in order to improve the sample quality. This was done by encapsulate a low meting point Bi−In−Sn alloy and prepared using the standard lift-out method at cryogenic temperatures [11].

2.3 APT sample preparation

2.3.1 Principles of the Focused Ion Beam instrument

Focused Ion Beam technology (FIB) is a well established technology for microscopy and micro and nano manipulation of almost any solid material. In a FIB, heavy primary ions are accelerated by an acceleration voltage to create a beam of ions. This beam is focused using a series of magnetic lenses and directed towards the material to be manipulated. The energy of the impacting ions may be so high that the bonding energy at the surface of the sample is overcome and the affected atoms are ejected away from the sputtered of the sample, milling away precise areas of the sample. This milling effect is the primary effect utilized in sample preparation of APT samples. The numbers of atoms that is sputtered off is material dependant, and is largely governed by the bonding energy in the material. The rate of sputtering can be controlled by controlling the acceleration voltage of the of the primary ions or the current density of the incoming ion beam [18]

There is other side effects of the impacting ions, they implant ions into the sample, altering the sample surface. The sputtered atoms can as well be adsorb back to the sample after sputtering. The ion beam impacting solidifies this deposited material as a side effect of the ion impacts, firmly redepositing the material to the sample in the area where the beam is focused. This effect can be used to purposely deposit films to the sample. By introducing film precursor to the sample through a gas nozle, purposely adsorbing precursors to surface. The ion beam can subsequently be used to trigger a reaction in the deposited precursors, solidifying the film and firmly adhere it to the surface. The process of milling and deposition are however competing processes and they both happen simultaneously when the sample is exposed to an ion beam, and their rate is largely determined by the acceleration voltage and current density. The rate of each process is shifted by altering the acceleration voltage and current density to favor the wanted process, in general depositions are made at a lower current density compared to milling. As a larger current density in a faster milling process a faster milling and gives the introduced gas less time to adsorb to the surface compared to the rate the material is milled away[18, 17].

Although the focused ion beam can itself be used as standalone and fully functional instrument. it is often coupled with an Scanning electron microscope (SEM) component in most modern instruments for imaging of the samples. The electron beam is places orthogonal to the ion beam as illustrated in figure this is done for several reason. Firstly because SEM have a higher resolution comapared to FIB[10] which makes it more suitable for imaging applications. The FIB does as well damage the sample. In addition to sputtering surface atoms the FIB does as well implant some of its primary ions into the sample. Even though these effects are highly dependant on acceleration voltage and current density and the damaging effects can be limited when imaging using lower voltages and lower current densities. They are always present to a degree. Longer exposure time which is necessary for high quality imaging also amplifies this effect. The electrons of an SEM carries a much lower energy and does therefore not damage the sample in this manner and is therefore far more suitable for high quality imaging[18]. The last major advantage can be considered as a positive consequence of the necessity of a second imaging component. It is very practical to have a second viewpoint orthogonal to the other, when manipulating complex 3D structures. This give the advantage of being able to accurately judge height and depth at the same time, without moving the sample.

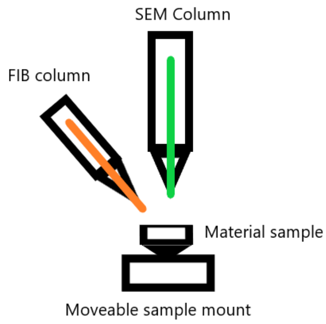

Figure 2.3: Simple illustration of the beam configuration for dual beam FIB/SEM instruments

2.3.2 APT sample prearations using FIB

FIB is today the most common method of sample preparation. FIB offers a precise method of preparing tips suitable for APT analysis. The main advantages of using this method is that it is possible to precisely manipulate the apex of the tip to the region of interest.The in plane sample preparation method used in this project is the most time efficient and easiest way to make APT using the FIB. As it is possible to extract several samples from the same liftout procedure. It is also easy to achieve a well aligned, vertical tip as the dug out samples are in the correct orientation for APT analysis without the need for rotation or complex geometric manipulations in order to place the samples on a post. This method does however require that region of interest is accessible from the surface of the material sample within a reasonable depth[4]. The other common sample preparation technique is electropolishing, where the tip is formed by gradual electrochemical etching. even though it is faster to prepare sample this way it offer little control of the apex in relation to the ROI and it requires conductive properties of the material[14]

The sample preparation starts by the deposition of a protective Pt layer as shown in fig 2.4, as the FIB uses Ga ions to image and mill the sample, it is likely that the sample will be damaged during the preparation process as rebouncing and redepostion mechanisms from the ion beam will be prominent during the digout procedure which will be done under a fairly high current. Another beneficial effect of a protective Pt will be that depending on the material used, Pt will in many cases show a strong contrast in SEM imaging. This will give a good reference point for determining the rate of milling and the depth of the milling done in later stages of the sample preparation process. If the material shows a similar contrast to Pt, other protective elements such as tungsten or similar deposition mixtures can be used for the protective layer. The depth of the layer can be varied between 100-500 nm depending on the depth of the region of interest and the amount of protection this will need. The width of the protective layer is normally set to be around to around 2.5 µm or as wide as the mounting post it will be placed on.

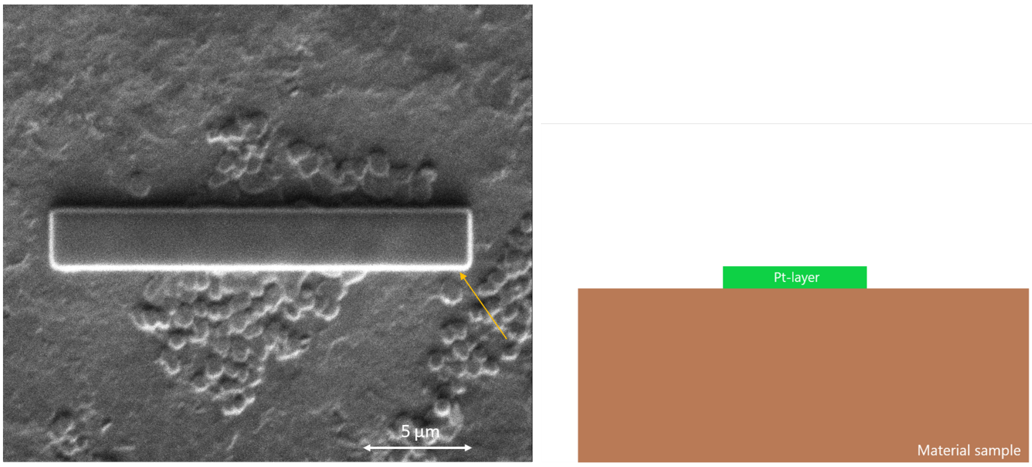

Figure 2.4: SEM and illustration of the applied Pt-protection layer, the yellow arrow points towards the applied Pt layer

After the proper protection layer is deposited the sample milling can start by digging two trenches on both sides of the protection layer. The trenches are typically milled at a 30 angle but this can be decreased or increased based on the depth of the ROI. The trenches are typically wide and are milled to the depth of where they intersect each other in the bottom of the sample slab as shown in fig **??**. After the trenches have intersected cleanup cuts are made, the cleanup cuts are made using a sequential cross-section that progresses the entire depth of the trench and sequentially moves towards the sides of the sample. This is done to eliminate damages done to the sample from redeposition and beam scattering due to the harsh milling conditions in the confined space of the milled trenches. It also ensures that the edges of the sample slab is sharp and defined, which makes it easier to align and fasten to the sample post later in the preparation procedure

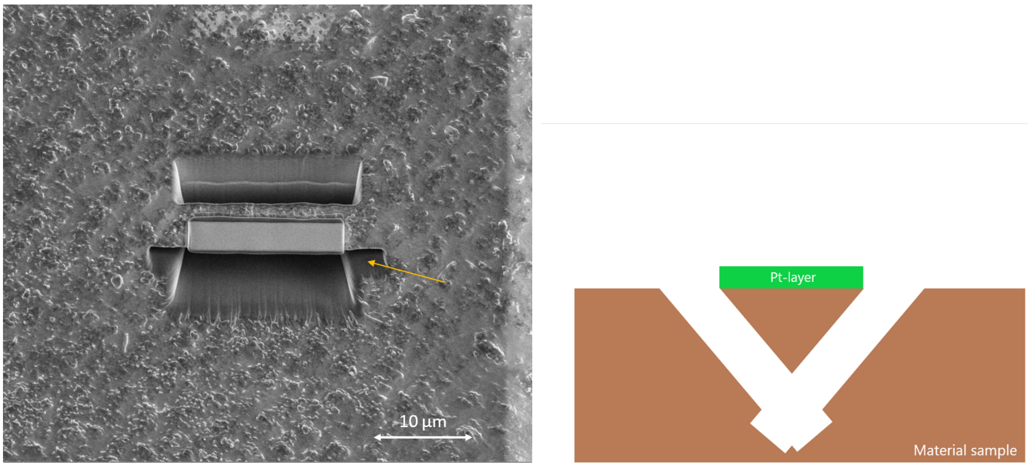

Figure 2.5: SEM and illustration of the milled trenches , the yellow arrow point to the side that have been cleaned using a cleanup cut

To lift out the sample slab one end of the slab towards the side where the lift out needle is inserted is milled clear from the surrounding walls and fastened to the lift out needle using a suitable deposition material. After the slab is sufficiently fastened to the needle the opposing side is cut free from the surrounding walls, the sample slab is at this point free from the surrounding material and can be lifted straight out and transferred to the coupon for splitting and tip sharpening. Image from the lit-out procedure and the coupon are shown in figure ??

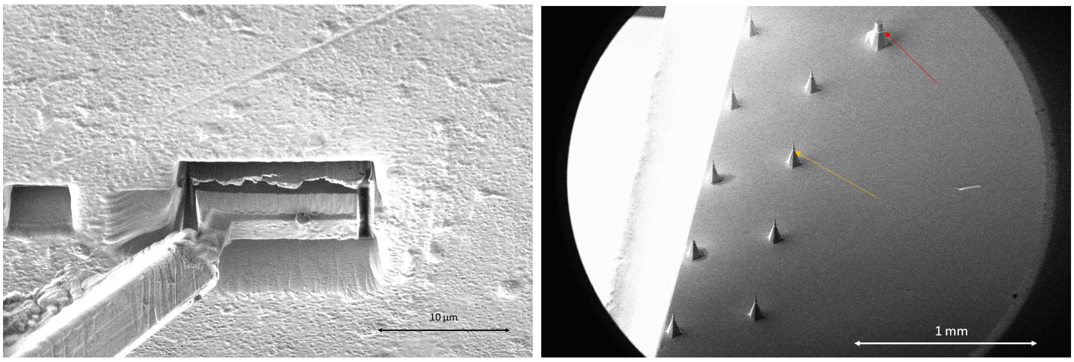

Figure 2.6: Image from the lift-out procedure to the left and an image of a samples coupon to the right, the red arrow indicates a navigation fiducial and the yellow arrow indicates a sample post

To split the slab in to sample sized chuncks the tip if the slab is positioned directly in the middle of the sample post and fastened with a Pt deposition in the crevasse between the flat post and the side of the sample slab. A sharp edge on the bottom of sample slab ensures a large surface area both on the post and on the sample to sufficiently fasten the sample securely to the post. Subsequently the end of the sample slab is cut leaving the long sample chunk on the post while freeing the rest of the slab to fasten to the next post. This procedure is repeated until the the slab is spent. After the slab is spent the stage is rotated and the backside of the sample chunks fastened with the same deposition procedure as the front of the sample. The fastened sample is shown in figure ?? along with an illustration.

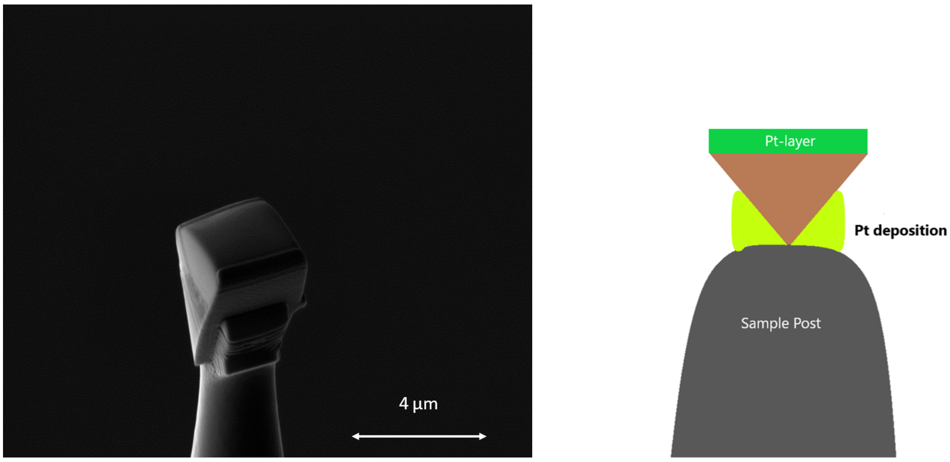

Figure 2.7: Sample fastened to a sample post with illustration

The samples are sharpened in to needles in several stages each using a progressively lower current to minimize damage and to promote a thin, and sharp needle about 50-100 um wide at the apex. The progression in the The initial stage is to flatten the area around the tip, this is to ensure that the needle to be formed is the only tip in the region of about 10 µm from the tip of the needle. This is done by milling a circle around the center of the tip, witch preferably is in the middle of the sample-chunk. With an inner diameter of 2 um and an outer diameter of around 4 um. The current used at this stage is not very important but and higher currents can be used to decrease the milling time. The resulting tip should be a 2 um wide cylinder with no secondary peaks around it as shown in fig ??.

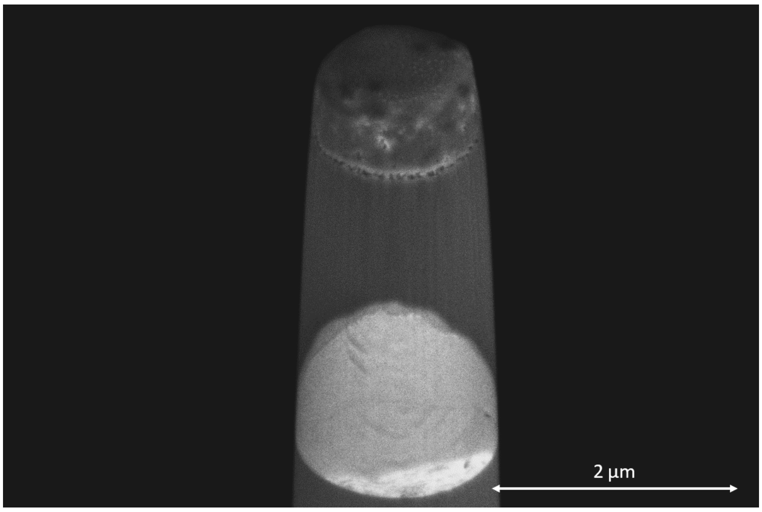

Figure 2.8: Sample shape after first milling stage of sample preparation

The tip shaping is done by reducing the inner diameter of the milling pattern to around 0,6 um, to push down the sides of the cylinder and leaving a thin but rounded needle, slightly wider in the bottom than on the top. In this step it is crucial that the milling is not done to long, as that will result in a cylinder, rather than a needle. The tapering characteristic of a needle shape in this step makes it possible to refine an apex in the next step. The resulting tip should be a fairly rounded needle with a tapering characteristic, about 0,6 um at the tip as shown in fig ??.

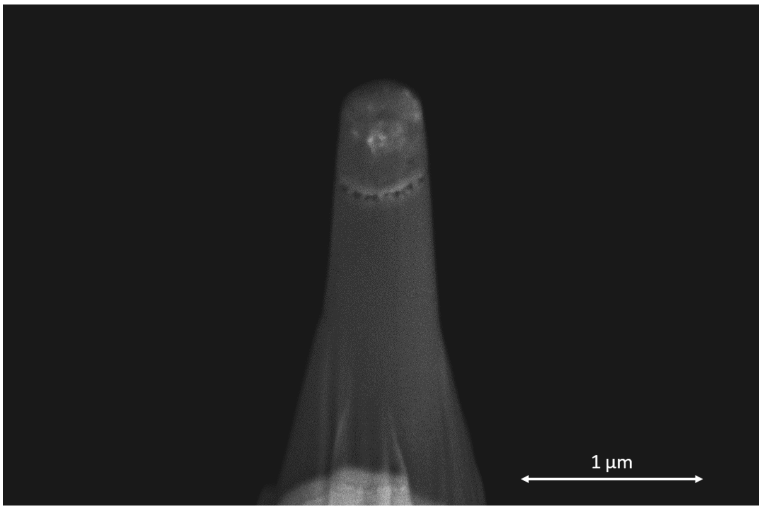

Figure 2.9: Sample shape after the second milling stage of sample preparation

In the final tip sharpening the aim is to make the tip as sharp and uniform as possible without losing the region of interest as shown in figure 2.10. The pattern diameter needed to reach a sufficiently low tip radius may slightly mill the center of the peak in addition the sides of the needle. This limits the amount of milling that can be done at this stage depending on how far down the region of interest is situated, and how much protective layer deposited on the sample. If the tip does not show signs of sharpening the inner diameter can be reduced but that will require a reduction of the milling current to avoid milling away the apex of the tip to quickly.

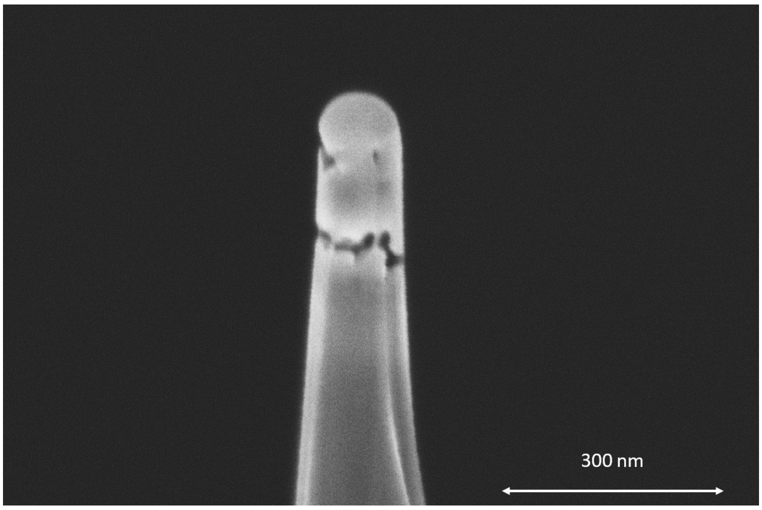

Figure 2.10: Sample shape after the second milling stage of sample preparation

Lastly, the tip is polished at a low voltage and a low current, this is typically done at 2-5 kV. The aim of this step is to remove the damaged layer on the surface of the needle, where the higher currents of the previous steps have implanted Ga into the material. The polishing is may also refine the tip slightly and is a good way to push the apex slightly down if the region of interest is a bit low in the needle from the previous steps. The time and size of this polishing step depends on how influential the damage layer is to the analysis but should be done from the top of the apex and down along to sides in order to not change the shape or blunt the tip.

3 Experimental

Instruments used during the project is given in table 3.1 along with their application. Specialized software utilized are given in table 3.2

Table 3.1: Table of instruments used and their application

Instrument	Manefacturer	Application
Helios Nanolab DualBeam FIB	FEI comapny	Sample praparation and imaging
LEAP 5000 XS Atom Probe	Cameca	APT analysis
3500 Series Diamond Wire Saw	Wells company	Cutting samples
Vacuum Classic 500 E-beam evaporator	Pleiffer	Deposition of Al/Ti protection Layers

Table 3.2: Table of specialized software used and their application.

Software	Developer	Application
IVAS	Cameca	APT reconstruction
NAPA	NTNU	APT data treatment
OVITO	Open source	3D rendering

3.1 Description of received samples

The samples analysed in this project was prepared and characterised by Marcus Soulm, as part of his master project spring 2020[16]. The substrates are of the alloy Ti6Al4V pre-textured by a high energy pulsing laser by collaborators in The group of Dr. Hermann Seitz , at the department of mechanical engineering and marine technology at the university in Rostok .The chemical compostion of the substrates are given in table 3.3[5]. The substrates was textured with 3 different patterns along with a polished reference sample. The different texture patterns are showed in figure 3.1. The fist textured sample is a LIPSS textured sample, annotated texture group L. LIPSS is an abbreviation of Laser induced periodic surface structures, and is a periodic nanoscale texturing where the laser ablates the surface and is rapidly moved across the material, with the aim to ablate a thin layer of the surface in a periodic pattern. The grooved sample textures are a microscale texture where the laser have been repeatedly ablating selected sections of the sample in a rectangular grid pattern, with an aim to repeatedly ablate and subsequently remove material from the exposed areas resulting in deeper groves. The final texture group of the samples are is the grooved ant LIPSS textured samples, annotated LG. these samples combine the two texturing methods in order to make a LIPSS textured surface in the space between the groves. The textured reference samples where given the annotation R.

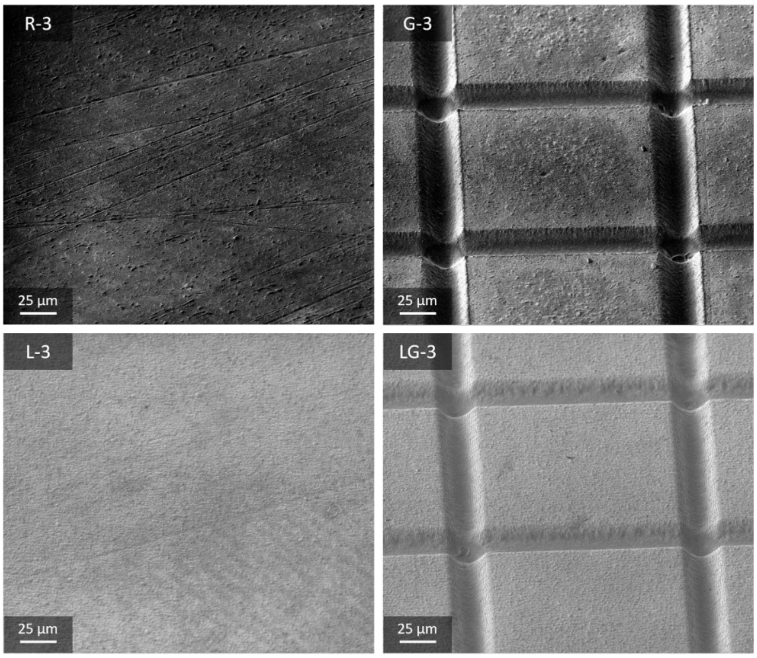

Figure 3.1: Overview of the different texturing for the provided samples[16].

Table 3.3: Maximum content for alloying elements for Ti6Al4V grade 5 titanium alloy[5]

	V	Al	Fe	O	C	N	Ti
wt. %	4,5	6,5	0,3	0,2	0,1	0,1	Balance
at. %	4,0	10,9	0,2	0,6	0,3	0,2	Balance

The textured samples was coated by Marcus Solum, using a sol-gel techunique with repeating rapid thermal processing. The precursor solution was prepared by an alcohol free modified abbreviation of the pechini method. Where a sol containing the $BaTiO_3$ precursours was prepared by mixing a $Ba(NO_3)_2$

solutuon with a Titanium-isopropoxide solution with a molar ratio of ${Ba_2}^+$ to ${Ti_4}^+$ of 1:1. This sol was spin coated on the substrates in 9 layers, heat treated between each layer application. The heat treatment program was reported to be the same between each layer applied and consisted of a 360 s ramp up time in air atmosphere to 700 °C .The sample was held at 700 °C for 360 s in air atmosphere before it was allowed to freely cool to room temperature in a pure nitrogen atmosphere[16].

3.2 preparations of APT samples

3.2.1 Cutting and lift-out procedure

All samples were prepared in a FEI Helios NanoLab DualBeam FIB, using the standard in-plane lift out method described in section xx. the Pt protection layer was deposited using a 30kv Ga-ion beam with a current of 0.28 nA with a y- dimension of 2,5 um, the x-dimension was varied depending on the number of samples to be prepared, the thickness of the Pt protection layer deposited varied between 0-800 nm, depending on the intended ROI. A lower ROI requiered a thiner protection layer. The trenches were dug at both sides of the protection layer at 30 with respect to the sample surface using a 30kv, 6,5 nA ion beam. The trench geometry had a length varied to the sample size, with a width of 3.5 µm and a z-dimension of 5 um or until the trenches where visually connected. The cuts were cleaned using a 30kv, 6,5 nA cleaning cross section until the Pt layer was in line with the edge of the sample bar as shown i figure 3.2

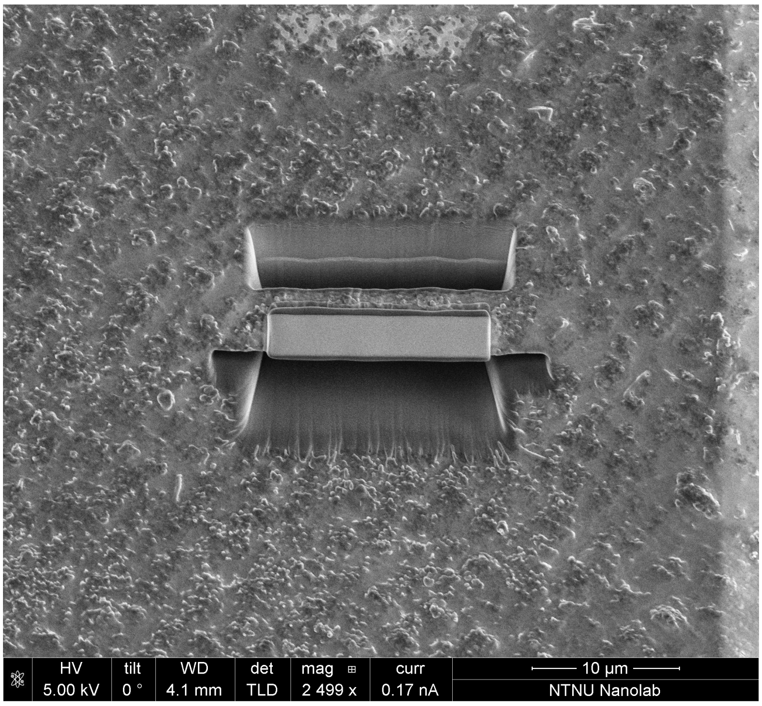

Figure 3.2: Image of finished trenches completely freeing the sample bar from the surface of the material sample, note the bottom trench is cleaned to be in line with the protection layer using a cleaning cross-section

The cantilever was cut using a 30kv, 6,5 nA beam with a rectangular pattern that did not overlap with the deposited protection layer. The lift out needle was attached towards the cut end of the cantilever using a Pt deposition with a 30 kV, 28 pA ion beam. The cantilever was subsequently cut free using a 30kV 0,28 nA ion beam and transferred to a sample coupon containing 22 sample posts.

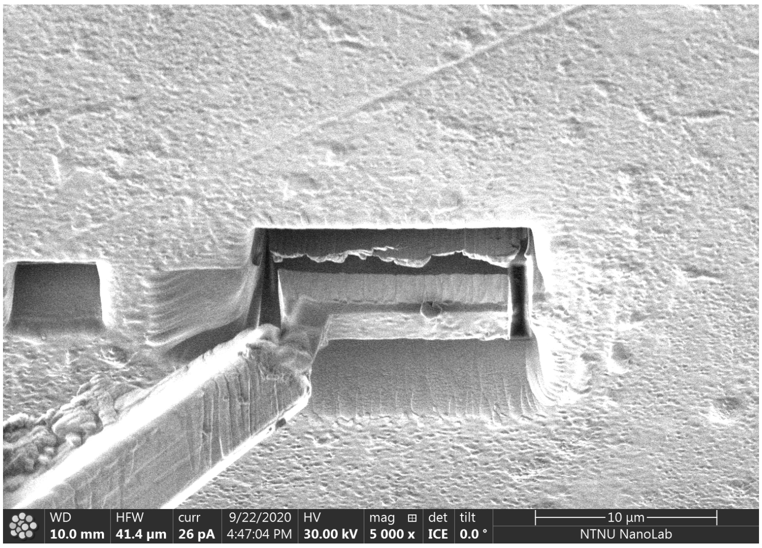

Figure 3.3: Free sample bar being lifted out using an Omniprobe lift-out needle.

The end of the sample bar was centered on the posts and fastened at the base of the sample bar with a rectangular Pt deposition using a 30kV, 28pA ion beam. After fastening the rest of the bar was cut free using a 30kV 0,28 nA ion beam as shown i figure 3.4. Leaving a sample on the post with approximately the same width as the post. This procedure was repeated until the remaining bar was split up and distributed on posts. The samples were then fastened on the backside using the same fastening procedure as initially described. Sample yield was estimated to be one sample per of sample bar.

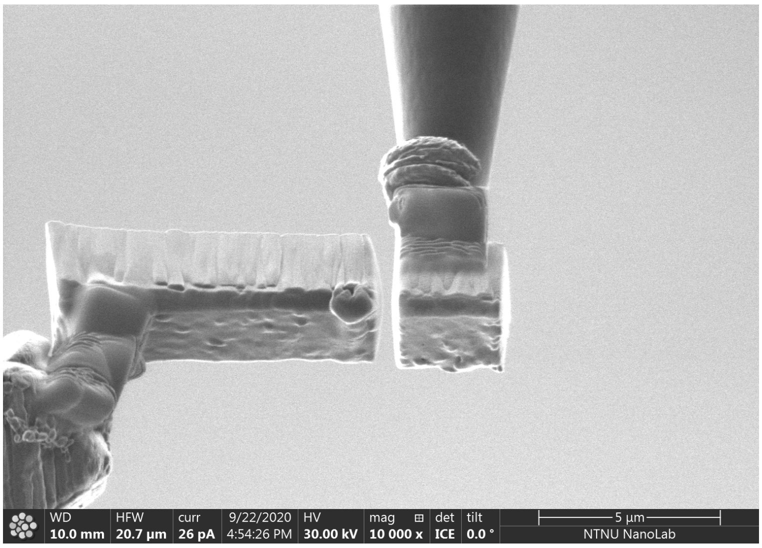

Figure 3.4: Sample mounting and subsequent cutting, the image display one sample mounted to the post and the remaining sample bar fastened to the lift-out needle to the left in the image

3.2.2 Sample shaping procedure

The first pushdown of the samples were made using an annular milling pattern centered around the middle of the post, with an inner diameter of 2 µm and an outer diameter of depending on the amount of excess material needed to be milled away. The milling was done at 30kv with a current above 0,28 nA. The milling was continued until the result was a single tip with a steep, smooth shank with no apparent bulges or protrusions, and a height difference between the primary apex and the closest secondary tips was more than 10 µm, as shown in figure 3.5. To achieve this it was sometimes necessary to increase the outer diameter of the pattern in cases where the samples where slightly tilted with respect to the ion beam. The resulting top of the sample was inspected to ensure a good and even Pt deposition on either sides of the sample base, as well as ensuring that the sample was positioned in the middle of the post as shown in figure 3.6.

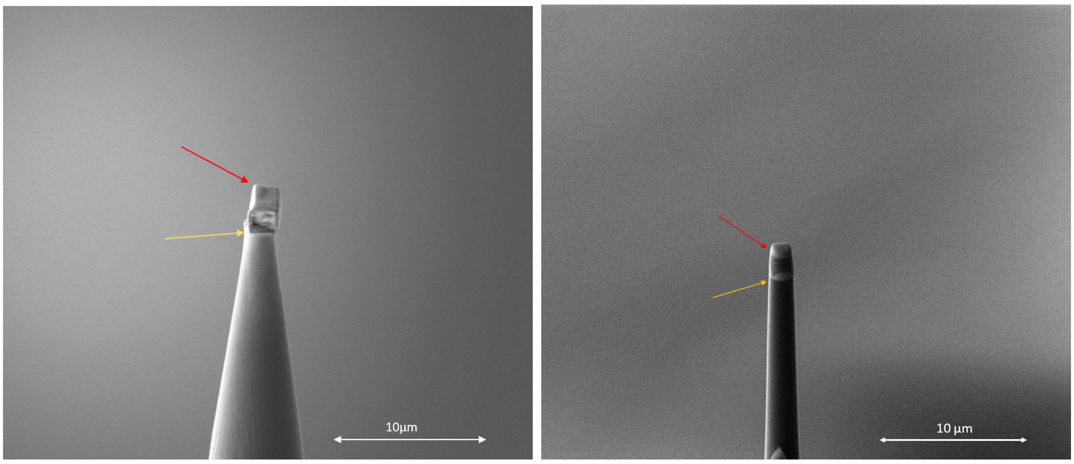

Figure 3.5: first stage of sample shaping, the red arrows indicate the fastened sample and the yellow arrows mark the start of the sample post. the image to the left show the sample on the post before milling and the image to the left show the sample after milling

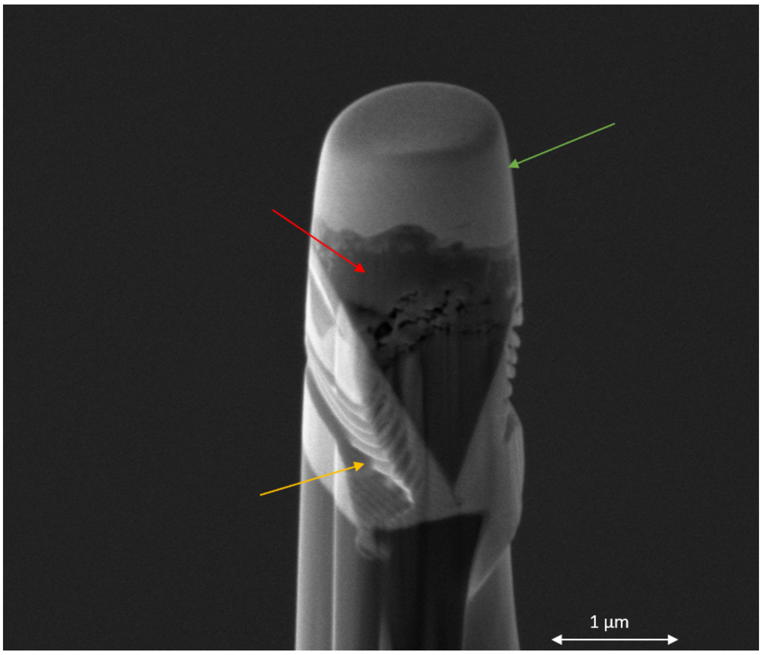

Figure 3.6: Closeup of the sample after the first stage of sample shaping, the green arrow indicate the Pt protection layer on top of the sample, the red arrow indicate the material sample to be analysed and the yellow arrow indicates the deposited Pt fastening the sample to the post.

Once the criteria described was achieved, the inner diameter was decreased to 0.6 µm and the outer diameter was decreased to match the base of the primary tip in order to not create new secondary peaks closer to the primary peak. The milling was done at 0.28 nA and continued until the the lowest point of the region of interest was no wider than 0.6 µm as shown in figure 3.7.

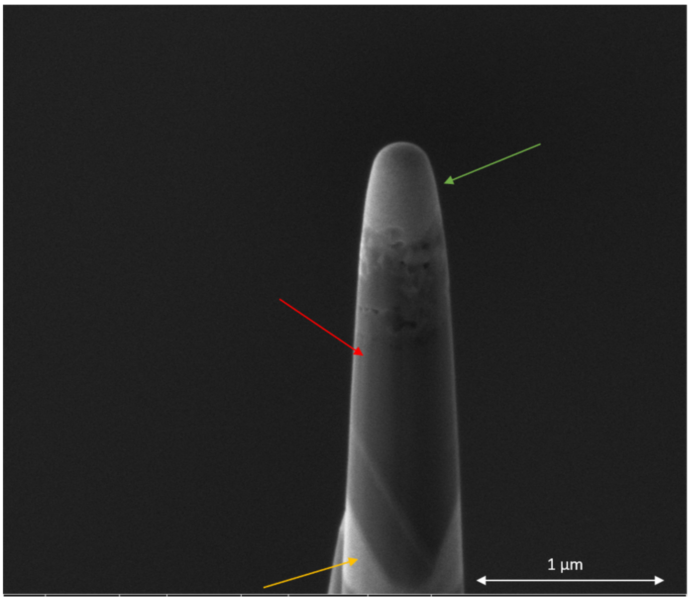

Figure 3.7: Sample shape after the second push-down of the sample, the green arrow indicates the applied Pt protection layer, the yellow arrow indicates the material sample and the red arrow indicates the Pt deposition fastening the sample to the post.

The final tip shaping was done by further decreasing the inner diameter to 0,3 um and milling at 0,28 nA until the apex of the tip had a diameter of less than 80 nm, as shown in figure 3.8.In cases where the tip was not sufficiently narrow the inner diameter of the pattern was gradually reduced down to 0,15 um along with a gradual reduction in milling current down to 28 pA. in cases where the apex of the tip was milled away before it had reached a satisfactory shape the milling current was reduced without reducing the diameter of the pattern until there was no visible milling of the apex.

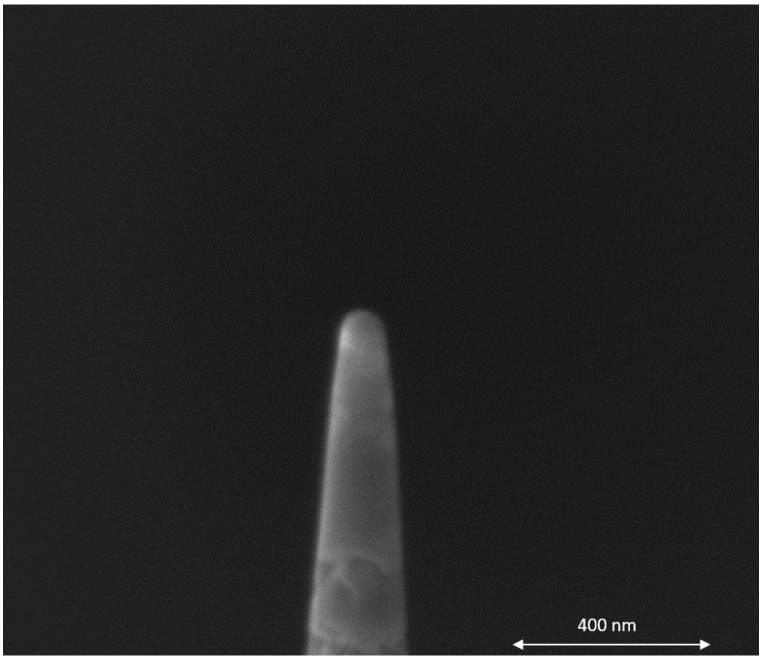

Figure 3.8: image of a finished prepared sample. Int this specimen there is no remnant protection layer left on the sample, and the mounting deposition is not visible in the image

After the desired tip shape was achieved the tip was polished using an annular milling pattern with an outer diameter of 4 um at 2 kV and 48 pA for 2-4 minutes or until the apex of the tip started to be pushed down. In cases where the apex of the sample was slightly to far above the region of interest, this step was used to deliberately move the apex of the tip down up to 40 nm before the procedure altered the shape of the tip to a degree that can be considered damage.

3.2.3 Deposition of Ti and Al protection layers

The primary material sample sample, L3 was quartered using a Wells 3500 Series Diamond Wire Saw with a 0.3 mm wire. The cutting procedure was done by fastening the samples to a sawing block with a water soluble, low melting point, Si-based wax. The sample cut twice in a crosshair pattern. The sawing was performed over 10 minutes for each cut. After the cut samples was successfully removed from the cutting block by melting the wax in lukewarm water, the samples were rinsed in water under ultrasonic vibration with a temperature of 45.C for 30 minutes. No damage to the film was observed upon visual inspection in SEM after the procedure.

Two of the quartered samples, L3-1 and L3-2 were respectively coated with a 300 nm Ti and Al layer in a Pleiffer Vacuum Classic 500 electron beam evaporator. The deposition rate was for both samples set to 1 Å/s for the first 100 nm of deposition and increased to 5 Å/s for the remaining 200 nm. Short time after the deposition, the coated samples where annealed on a hot plate set to 100 C for 4 hours. The resulting protection layers was observed to be fully adhered to the sample without visual pores or irregularities at the interface as shown in figure 3.9. APT samples prepared from the protected samples, where prepared with the same lift out and shaping procedure as the rest of the samples.

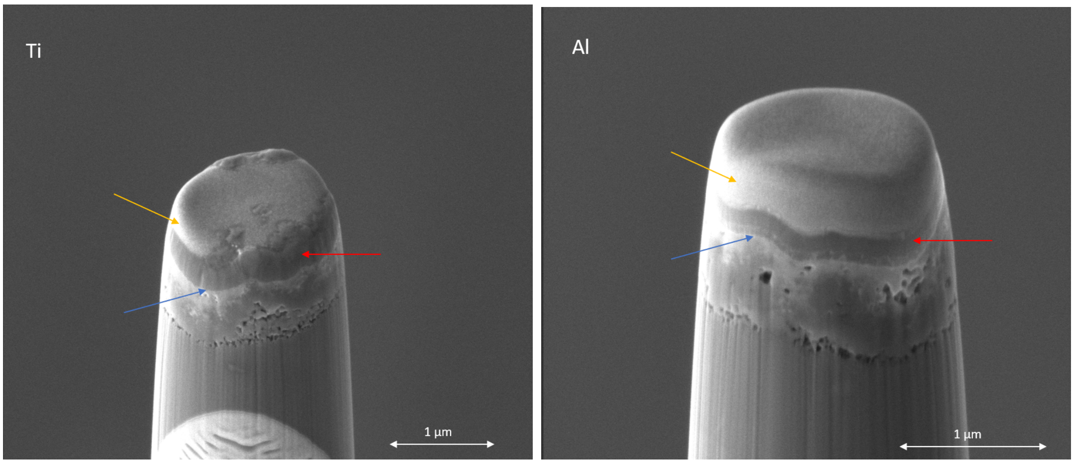

Figure 3.9: Images from the first shaping step of samples with a deposited Ti (right) and Al (left) protection layer. The yellow arrow indicates the Pt protection layer, the red arrow indicates the respective deposited protection layers and the blue arrow indicates the transition between the deposited protection layer and the surface of the material sample.

3.2.4 Deposition soldering of porous interfaces

Some samples which exhibited a highly porous interface region were soldered by a Pt deposition across the porous region using a 10 kV 86 pA electron beam. The deposition time was between 15-30 seconds. The soldering was done towards the end of the final tip shaping and excess Pt was easily milled away during the last stages of tip shaping and polishing. Samples suitable for soldering showed a initially narrow and defined region of porosity with a dense and structurally sound region above and bellow the soldered area. a comparison of a sample before and after soldering are given in figure3.10. A total of 4 samples where soldered in this manner.

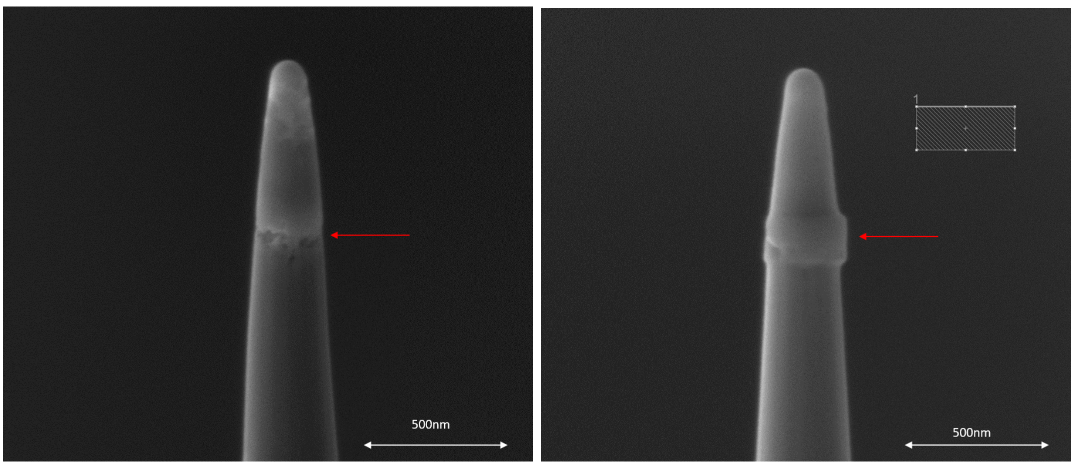

Figure 3.10: Pt soldered samples before and after the soldering.The left figure display the porous area before soldering, the right image show the same sample after soldering, before polishing. The red arrows indicates the porous and soldered region respectively.

3.2.5 Selection of ROI

From cross sections of the samples like the one shown in figure 3.11 the applied coating was determined to be above the distinct region with a high porosity. The porous region itself was identified to be the interface. This porous region is marked with red arrows in figure 3.11. The samples was prepared in such a way that the apex of the tip was placed above but as close to the intended ROI as possible. The intended ROI changed during the course of the project and was initailly placed just above the the porous interface line. During the progression of the project this ROI was gradually moved upwards, closer to the surface. Samples that had the ROI placed very close to the porous interface line with the intent of only analyzing the coationg material within 100-200 nm around the interface is annotated as a low ROI, and is marked with blue triangles in figure 3.11. Samples that were prepared with an ROI placed closer to the surface with the intent of analyzing a significant part of the coating layer of the sample, are annotated as having a high ROI and are marked with yellow triangles inn figure 3.11.

Figure 3.11 also show the the variation in porosity between L and R textured samples. The areas with a low degree of porosity highlighted by the green arrow, where targeted as suitable areas for sample preparation. This was achieved by orienting the milled trenches and subsequently extract the bar of samples going across the periodic texturing, ensuring the sample bar contained both valleys with a low degree and porosity and ridges with a high degree of porosity. Efforts where made during the splitting and distribution of the sample bar to the posts to match a region of low porosity to the center of the post. The primary effort made was matching the separation cut with an area displaying a high degree of porosity, consequently aligning an area with low degree of porosity to the middle of the sample post.

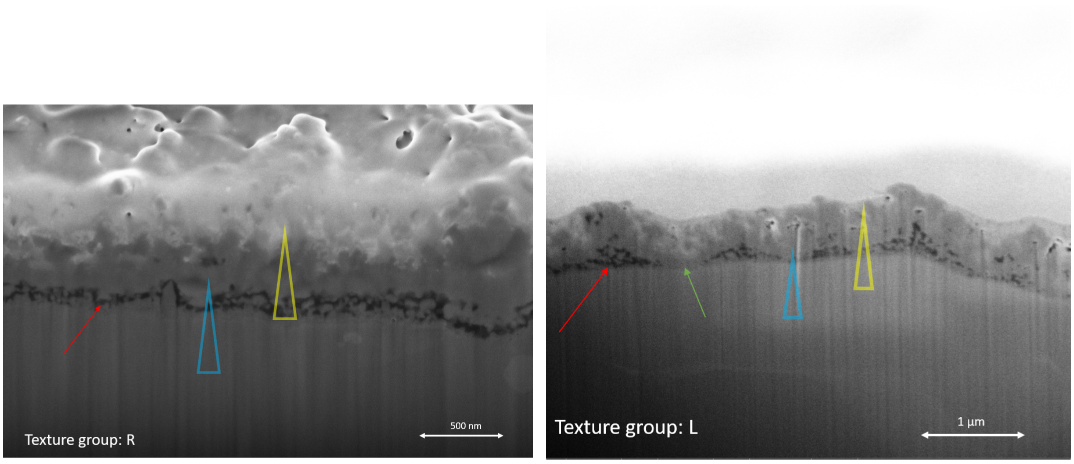

Figure 3.11: Crosssection of samples with texture group R to the left and texture group L to the right. The red arrows indicates the porous region interface region, the green arrow highlights an area of relative low porosity only present in texture group L. The triangles indicates the ROI as a targeted position of the prepared APT samples. The blue and yellow triangles indicates the low and high ROI respectively

3.3 APT Analysis parameters

The samples was analysed using a Cameca LEAP 5000 XS Atom probe, with a linear flight detector. The range for different key analysis parameters are given in table 3.4. The chamber temperature for analysis was increased from 25K to 50K over the course of the project. The detection rate was set between 0,3 and 1% where 0,5 was used in the majority of the experiments. A detection rate at 1% was only used early in the project. The pulse energy was varied by in-situ evaluation based on resolvability of the evolving mass spectra. The pulse energy was in the majority of the analyses set to 60 pJ. In instances where the applied voltage increased rapidly short time after the initiation of the analysis, the pulse energy was increased up to 130pJ. The pulse frequency was set to 250 kHz, Lower and higher pulse frequencies was tested with no apparent effect on the obtained mass spectra. The initial applied voltage necessary for evaporation to occur was typically between 3-5 kV. Fracture occurred at an applied voltage between 10-11 kV for successfully analysed samples. The produced data was recontructed using IVAS, a reconstruction software issued by the manefacturer of the instrument. Data treatment was done using an unpublished alpha version of NAPA, a data treatment software internally developed at the institute for material sciences at NTNU.

Table 3.4: Table showing the range of analysis conditions used.

Pulse method	Detection rate (%)	Temperature (K)	Pulse energy (pJ)	Pulse requency (kHz)
Laser	0,3-1,0	25-50	30-130	200-250

4 Results

4.1 APT results

4.2 Eralier charceterisation of the samples

The received material samples had earlier been characterised by Marcus Solum. Using different characterisation techniques . The results of the relevant characterisations previously performed on the samples are recounted in this sub chapter[16]. Figure 4.1 show the obtained XRD difractogram for the coated samples for all 4 texture groups as reported by Solum[16]. The phases present in the difractogram was determined to be rutile and anatase TiO_2, $BaTiO_3$, Barium aluminium titanium oxide and the substrate Ti6Al4V. The results from the EDS line scan are shown in figure 4.2. and show the meassured evolution of Ba,Ti,O,Al and V for the indicated line

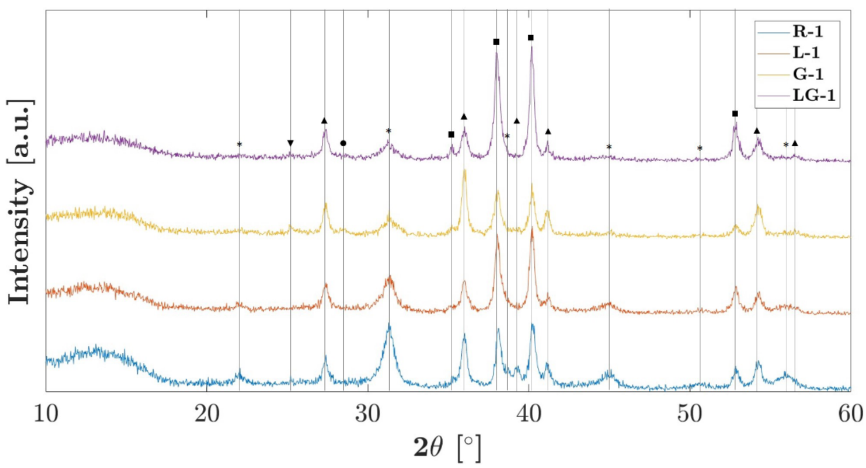

Figure 4.1: XRD as reported by Solum. The peaks are marked as follows: (*) for BaTiO3, (■) for TiAl10V4, (▲) for rutile TiO_2 ,(▼) for anatease TiO_2 and (●) for Barium aluminium titanium oxide [16].

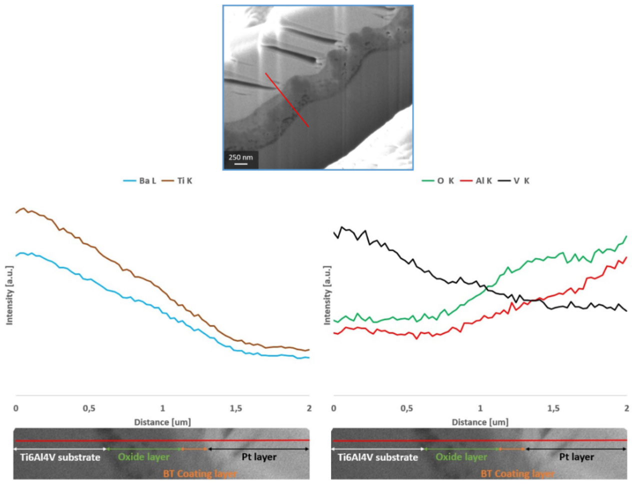

Figure 4.2: Redults from EDS line scan as reported by Solum [16]

4.3 Evaluation of prepared samples

All the prepared samples are listed in table 4.1 along with a brief description of their characteristics aswell as special sample preparation procedures applied to the sample. Not all of the samples where attempted analyzed. The discarded samples where discarded based on an evaluation of their deviation from intended shape or ROI , degree of porosity and an evaluation of their possibility to provide new data. All the analyzed samples are listed in table. the analyzed samples are listed in table 4.2. Figure **??** show a representative selection of samples that where discarded and not attempted analysed based on their characteristics of either being deemed to porous, have a drastically abnormal shape or a clear loss of ROI.

The analyzed samples are listed below in table 4.2. A low amount of the totally produced samples were analyzed successfully. The primary evaluation criteria for a successful analysis is the amount of data collected, this is given as the number of impacts on the detector during the analysis. for the application of interface studies, the length of the sample analyzed is crucial in order to get a coherent and uninterrupted picture of the evolution of species throughout the sample. For the application of the interface studies a thin film analysis a minimum z-direction of 200 nm was deemed sufficient in order utilize the results in a meaningful way. Samples that did not emit a sufficient amount of ions to achieve this before fracture, or were truncated for reasons such as asymmetrical evaporation, fluctuations in detection rate or loss of ROI. Was consequently not deemed a successful analysis for this application.

Another evaluation criteria for a successful analysis is a continuous evolution of the sample. Where the needle is gradually evaporated from the tip and progress down with a single apex with no smaller fractures or splitting of the apex. Smaller fractures or flashes as a result of species with a large discrepancy in ionization energies, results in a rapid fluctuation in detection rates and subsequently a rapid increase or decrease in field strength necessary to maintain a constant rate of evaporation. under the analysis of an ideal sample the field strength should gradually increase as the apex of the tip progressively becomes wider and the shank angle increases. Samples that did not show this behavior but rather had random increases or decreases in necessary field strength was deemed unsuccessful on the basis that the results would not be continuous, and the data would not be usable for the application of either interface or thin film studies.

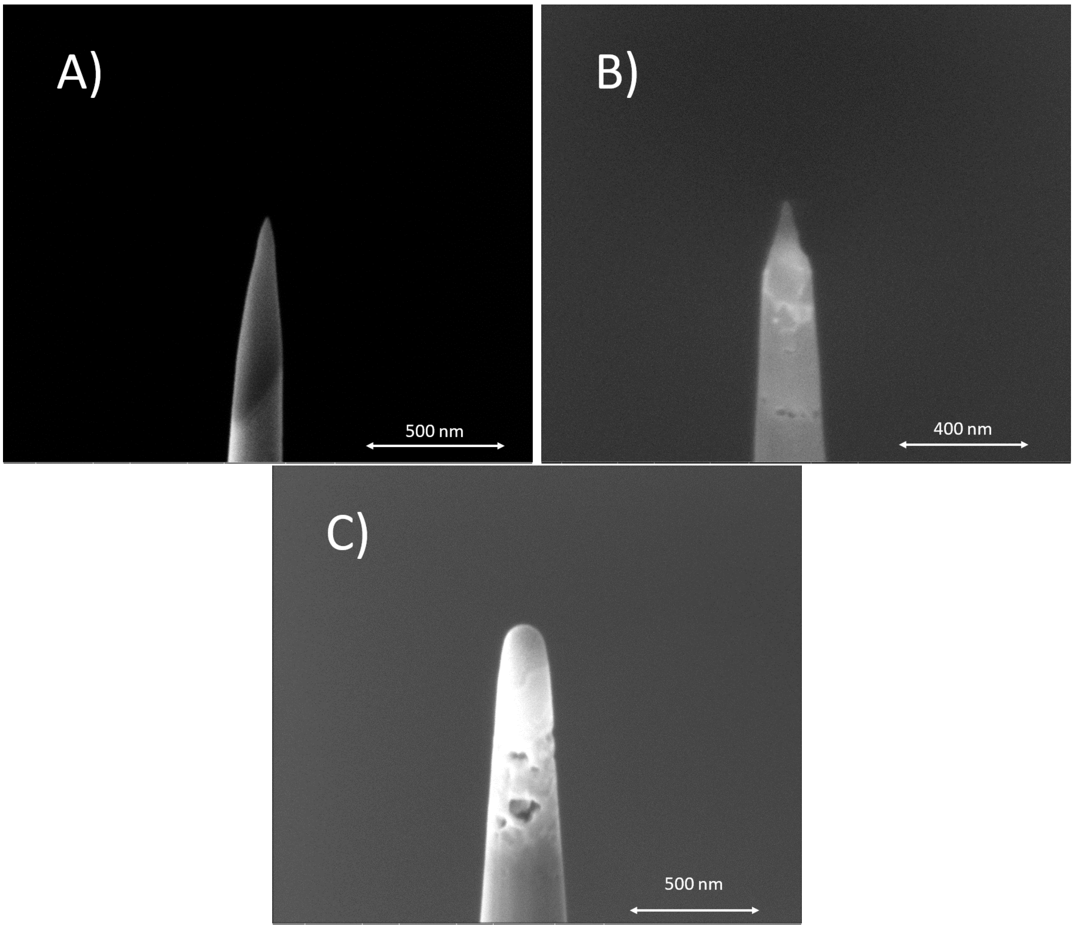

Figure 4.3: representative selection of discarded samples. sample A) have a clear loss of ROI, sample B) show a drastically abnormal tip with varying shank angle and sample C) is too porous for analyis.

The last criteria for a successful analysis were that the intended region of interest was present in the sample. During preparation of samples with an apex < 100 nm the low contrast in SEM makes it hard to precisely judge the position of the tip relative to the intended region of interest. The porous nature of the coating also poses further challenges in this regard as the tip would deform or collapse because of pores in the sample. These samples required further milling to reach an acceptable shape and in many cases this led to a loss of the region of interest. Porous samples also pose an increased risk of damage during handling and transport post preparation. Where whole sections of the sample may fall off or in other ways be damaged by the process of transferring the sample to the atom probe. Samples with a lost region of interest was identified from the lack of compositional evolution during the initial parts of the analysis, from high initial field strength or from an observed composition equal to that of the expected substrate composition.

4.4 Results 1D profile and 3D reconstruction from highest quality sample

Sample L3-17 provided the longest and most compete data set obtained from one singe sample. This sample was prepared utilizing a Ti protection layer and displayed a low amount of porosity.The obtained mass spectra is shown in figure xx The analysis was performed at 50K and the total amount of impacts obtained during the analysis was 1,06 e9 impacts. This yielded a total analysed length in Z direction of 1,2 um. A 3D representation along with the original of the first 400 nm of the sample is given in figure

4.4 bellow for the selected major component of ions: Ti^{2+} , TiO^{2+} and TiN^{2+}. As shown in the figure 4.4 bellow, the TiO^{2+} is situated towards the top of the sample. the TiN++ is found mostly in between the TiO^{2+} and Ti^{2+} regions.

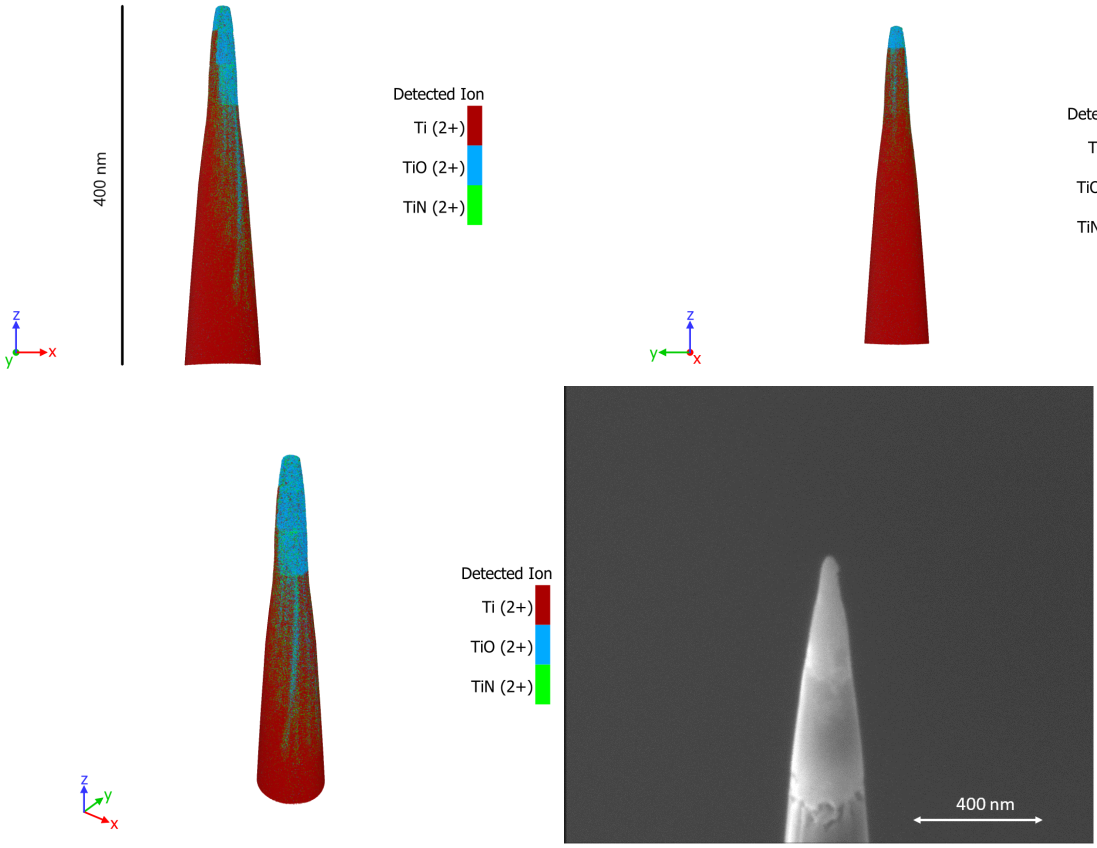

Figure 4.4: 3D reconstruction containing the 3 most prevalent ions detected from sample L3-17. The same sample is represented from 3 different angles along with a SEM image of the analysed sample.

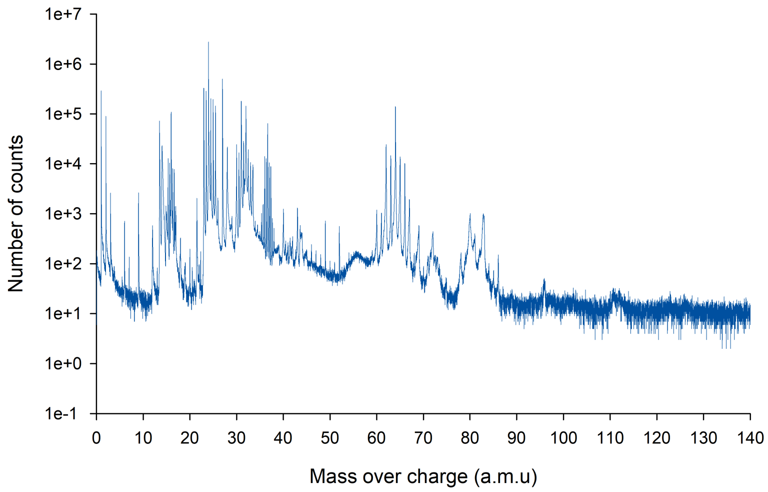

Figure 4.5: ombtained mass spectra form sample L3-17

This sample was also utilized to construct an atomic 1D concentration profile of the sample, shown in figure 4.6. the 1D concentration profile is constructed from a 10nm radius sample cylinder stretching the entire sample length of the sample in the z-direction. The 1D composition profile in figure 4.6 show the evolution of the different species present in the sample from the start of the analysis at 0 nm, towards the bulk composition to the right in the composition profile. As shown in figure xx there is an initial high amount of oxygen towards the surface in the sample which decreases towards the metallic interface at around 430 nm and subsequently stabilize at the expected bulk composition for the substrate. The Nitrogen contribution increases and stabilize at about 20 at% between 150nm the metallic interface at 410 nm.. The relative amount of vanadium remains relatively constant throughout the sample volume but does exhibit an accumulation just above the nitrogen rich region in the coating. The relative aluminum content decreases towards the top of the sample. The barium content is significantly lower than can be expected from a $BaTiO_3$ coating, with a maximum barium content towards the top of the sample at 05 at%

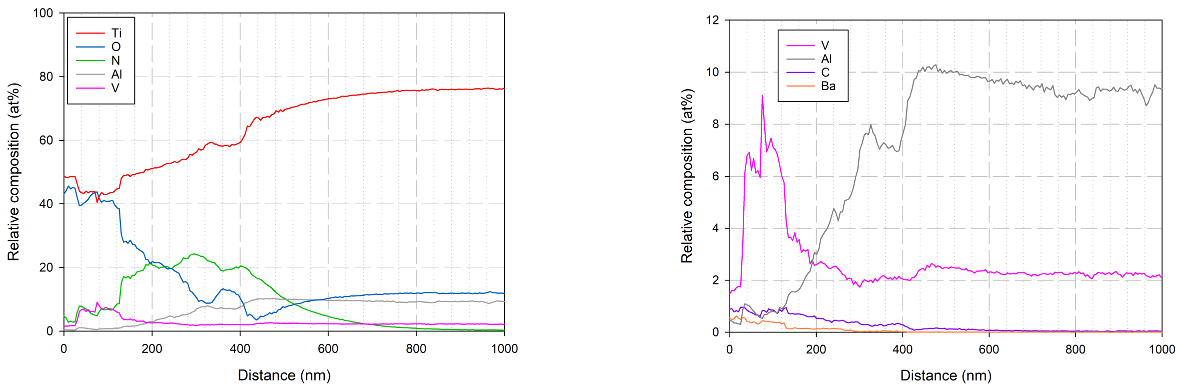

Figure 4.6: 1D profile from sample L3-17, produced with 5 nm resolution

4.5 Results from other successfully analysed samples

The other successfully analysed samples did not provide as complete data sets as L3-17. Their analyzed volume was smaller and their placement relative to the surface or the interface of the sample is obscure. A 1D concentration profile of the samples R3-2, L3-2 and L3-12 is given in figure 4.7. R3-2 is a sample made from texture group R, with a low ROI and subsequently only show a region close to the interface. L3-2 similarly also show a region close to the interface for a L textured sample. Sample L3-12 was a sample prepared with a Ti protection layer and show a region somewhere in the coating layer of the sample. No Ba was found in any of these samples. the carbon content is not displayed and was found to be bellow 1,0 at. % in all 3 samples. No 3D reconstruction was made from these samples. Images from all 3 samples are displayed in figure 4.8.In addition, bulk BT samples where briefly tested and used to verify the correct pulse frequency for detection of Ba. They where however not analysed long enough to obtain any significant volume that could be reconstructed.

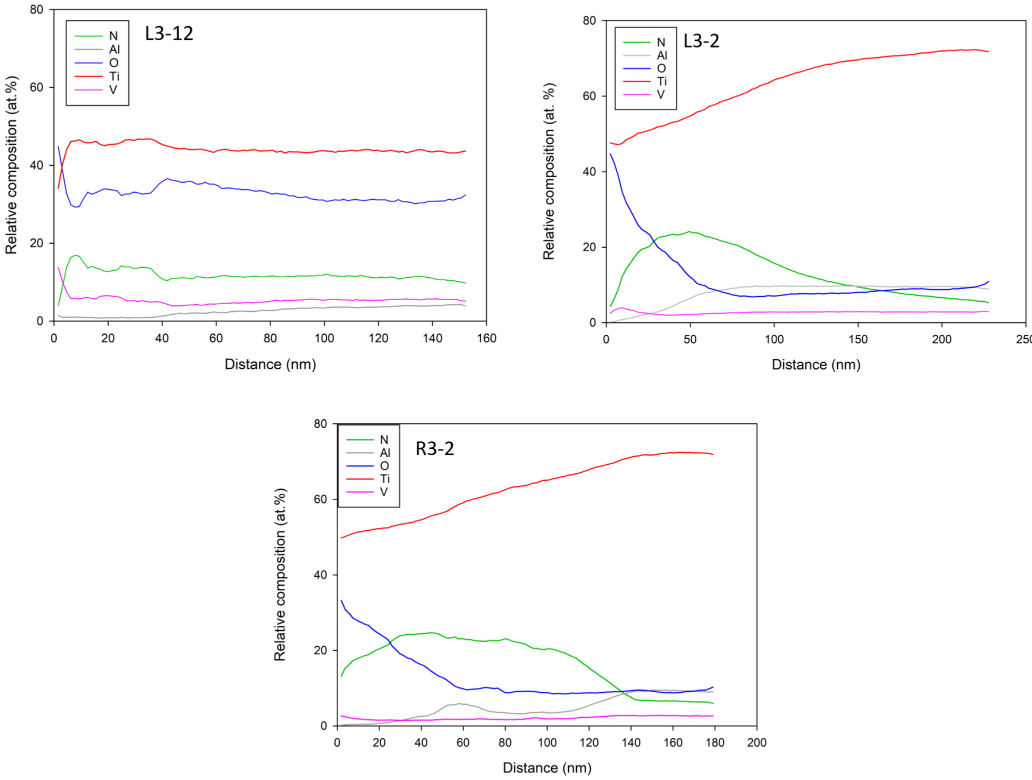

Figure 4.7: 1D concentration profiles calculated from samples L3-12, L3-2 and R3-2

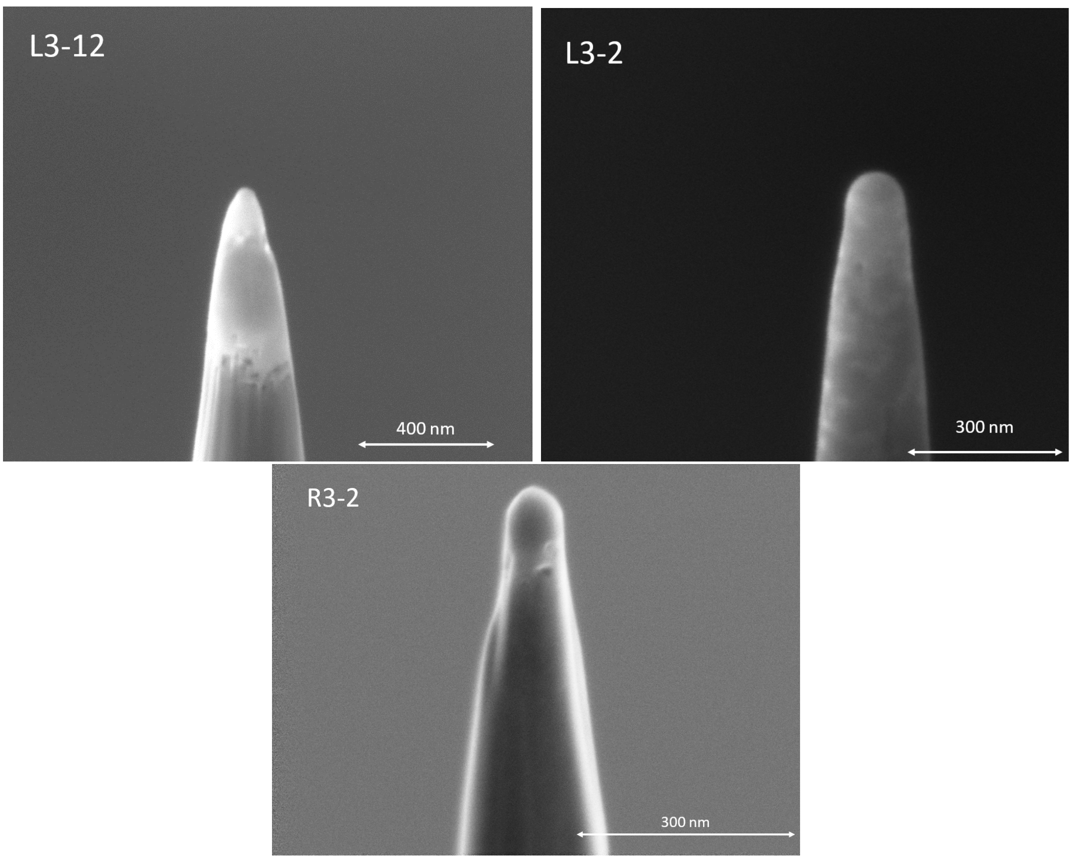

Figure 4.8: Images of the sucsessfully analysed samples: L3-12, L3-2 and R3-2.

Table 4.1: Table of produced APT samples in order of production

Sample name	Parent sample	Pt-soldered	Remnant protection layer	apex diameter	ROI Depth (high/low)	porus area (loctaion)
R3-1	R3	no	none	80 nm	low	none
R3-2	R3	no	none	50 nm	low	interface
R3-3	R3	no	none	40 nm	low	interface+ coating
R3-4	R3	no	none	90 nm	low	interface
R3-5	R3	no	none	100 nm	low	upper
R3-6	R3	no	none	40 nm	low	upper
R3-7	R3	yes	none	80 nm	low	interface
R3-8	R3	yes	none	100 nm	low	interface
R3-9	R3	no	none	80 nm	high	interface
R3-11	R3	no	none	70 nm	high	high
R3-12	R3	no	none	100 nm	high	none
R3-13	R3	no	none	70 nm	high	interface + coating
R3-14	R3	no	none	80 nm	high	interface
R3-15	R3	no	none	50 nm	high	interface
L3-1	L3	no	none	20 nm	high	none
L3-2	L3	no	none	70nm	high	none
L3-3	L3	yes	none	90 nm	high	interface
L3-4	L3	no	none	100 nm	high	interface
L3-5	L3	no	Pt	30 nm	high	interface+coating
L3-6	L3	no	Pt	40 nm	high	none
L3-7	L3	yes	Pt	40 nm	high	interface+coating
L3-8	L3	no	Pt	30 nm	high	coating
L3-9	L3	no	Pt	70 nm	high	coating
L3-10	L3	no	Pt	100 nm	high	coating+ interface
L3-11	L3	no	Pt	80 nm	high	interface
L3-12	L3	no	Ti	30 nm	high	interface+ coating
L3-13	L3	no	Ti	60 nm	high	interface
L3-14	L3	no	Ti	80 nm	high	none
L3-15	L3	no	Ti	60 nm	high	interface
L3-16	L3	no	Ti	40 nm	high	interface
L3-17	L3	no	Ti	20 nm	high	interface
L3-18	L3	no	Al	60 nm	high	interface
L3-19	L3	no	Al	90 nm	high	interface+coating
L3-20	L3	no	Al	60 nm	high	none
L3-21	L3	no	Al	60 nm	high	coating

Table 4.2: Table of the analyzed samples with remarks

Sample name	Number of impacts	T (K)	Detection rate (%)	Remark
R3-1	1,00E+07	25	0,5	ROI lost, substrate
R3-2	3,90E+07	25	1,0	Successful analysis
R3-3	2,10E+06	25	1,0	Rapid fracture
R3-4	2,00E+06	25	1,0	Rapid fracture
R3-6	1,35E+07	25	1,0	Truncated, ROI lost
R3-7	1,00E+06	25	1,0	Rapid fracture
R3-8	1,00E+06	25	1,0	Rapid fracture
L3-2	9,10E+07	25	0,5	Successful analysis
L3-3	7,00E+05	25	0,5	Rapid fracture
L3-4	8,30E+06	25	0,5	Short run, truncated
L3-5	9,00E+05	25	0,5	Rapid frature
L3-6	1,80E+05	25	0,5	Rapid fracture
L3-7	1,50E+06	50	0,5	Rapid fracture
L3-8	3,00E+05	50	0,5	Rapid fracture
L3-12	1,20E+07	50	0,5	Sucsessfull analyisis
L3-13	6,70E+07	50	0,5	Sucsessfull analysis
L3-17	1,06E+09	50	0,5	Sucsessfull analysis
L3-18	2,00E+06	50	0,3	Rapid fracture
L3-19	1,00E+05	50	0,3	Rapid fracture
L3-20	3,80E+05	50	0,3	Rapid fracture

5 Discussion

5.1 evolution Concentration profile

From the 1D concentration profile of sample in figure 4.6 two main regions can clearly be identified: the original substrate and the material applied as a part of the coating. The coating-substrate interface is determined to be at around 410 nm, where the evolution of the different species follows a predictable behavior, consistent with that of diffusion in a dense metal. The applied coating region, found before 410 nm can further be split up in two distinct regions; one with a high amount of TiN or TiN_2, and one which primarily consist of TiO_2.The oxygen concentration drops off across the nitrogen rich region between 130 and 430 nm, while the concentration of Nitrogen remains relatively constant just above 20%. The very top of the sample, above 130nm primarily consists of TiOx. This region also contains a high amount of vanadium between 7-9 at% which is substantially higher than the bulk substrate composition at 2 at%. It is also in this region the concentration of Ba starts to increase from 0 at% up to 0,5 % at the very tip of the sample. the very top TiO_2 region is for these reasons determined to be the start or the entirety of the intended$BaTiO_3$ layer in the sample.

5.2 Quality of the 1D concentration profile

When evaluating the validity of the 1D concentration profile in figure 4.6, the first aspect to address is the sharp and abrupt changes in the coating area, above 420 nm. The most apparent abrupt change in this region is the sudden shift in composition around 130 nm. In this region the oxygen and vanadium rapidly drop off along with an increase of nitrogen equivalent to the drop off in oxygen. This abrupt behavior is unexpected and may be an indication that a small fracture in the sample occurred above this region where a portion of the coating layer was fractured off. If this is the case the quality and validity of the produced concentration profile would be drastically impacted as it can no longer be regarded as a continuous and uninterrupted representation of the depth evolution in the sample.

The 1D profile was made sampling a smaller and narrow volume of the analyzed sample. From the analyzed volume a smaller cylinder with a 30 nm diameter was used as the basis of the 1D profile. A 30 nm cylinder was chosen as this is the calculated diameter of the apex of the sample, making the sampled cylinder as large as possible without varying the total amount of sampled ions in the top of the cylinder compared to the lower regions.

This has the benefit of eliminating the influence of the misalignment between the orientation of the region of interest and the sample direction. As seen in the 3D representation in figure 4.4 the interface region is not perpendicular to the z axis of the sample. If the concentration profile had been based on the entire sample volume, this misalignment would lead to different regions of the sample being sampled together in the same z-bin and subsequently misrepresent the composition and size of the different regions in the sample to a point where they are indistinguishable from each other.

A reduction in sample volume does however increase the influence of local variations which is not representable for the material investigated. Small abnormalities, such as nanosized pores or local concentration increases which in other instances would have been evened out by an increased sampling volume will have a large impact on the results. To limit the impact of error like this the cylinder was made as large as possible while still retaining a uniform density throughout the cylinder as earlier described.Another factor to consider is that the analysed area of the material sample that is very small, only about 20x20 nm. It can therefore not be considered a universal representation of the entire material sample. To obtain a more statistically representative picture of the compositional evoultion in the sample as a whole. Data from several APT samples needs to be considered together. Preferably taken from random point in the material sample, which was not possible in the L3 material sample because of the specific regions with high and low porosity.

The abrupt changes in composition can as well be amplified by drastic changes in the field of evaporation for the different material compositions. As the field of evaporation is remained as a constant parameter for a certain region of the sample in the reconstruction protocol. This is inherent weakness of the method when performing interface studies and the effect is most apparent when the discrepancy in evaporation field is large and is expected to happen when large shits in composition happens over a short distance[2].

5.2.1 Compositional evolution of titanium

As Ti is expected to be present in both the Bt coating and the substrate, the compositional evolution of this element is not the best element for defining different regions of the sample. It does however constitute the majority of the sample volume. As shown in figure 4.6 The Ti follows an increasing behavior from the surface of the sample towards the bulk of the substrate, where it stabilizes at around 75%. In the intermediate N rich region the Ti concentration steadily increases. The fact that the N remains constant and the O decreases indicates that the amount of unbound Ti increases at the expense of TiO. At around 100nm there is a slight dip the the relative amount of Ti this indicates the presence of a phase that does not contain Ti and corresponds to the increase in V found in the same region, this will be further investigated in the discussion about V. The fact that Ti is expected to be found in all regions of the sample with overlapping phases and constituents makes stochiometric analyses difficult to utilize in order to determine the compositions of the different phases present in the sample.

5.2.2 Compositional evolution of Nitrogen

The nitrogen concentration rapidly increases at around 130-140 nm. Nitrogen is not a part of the intended constituents of the smaple but was introduced as a part of the synthesis process under the annealing of the samples wich was done in under pure nitrogen atmosphere. This was done in order to reduce the growth of the expected TiO inter-layer which was deemed unbeneficial for the samples by Marcus Solum. As no comparison between a sample annealed in air and a sample annealed under nitrogen gas is made it is not easy to definitively determine the effect of this treatment or if it achieved its intended purpose of decreasing the size and porosity of the inter-layer. It can however be observed that the N has accumulated between the TiO and the possible $TiBaO_3$ layer. It also drastically impact the amount of O present in the area. as the O concentration drops bellow that of the bulk composition over this region. This indicates that the Nitrogen indeed limits the growth of TiO the nitrogen concentration does

This accumulation of N is likely in the form of TiN, as if it would have been present in the form of adsorbed N_2 there would likely have been observed as ions of N^+ or N_2 rather than TiN^+. from the 3D Reconstruction in figure 4.4 it does as well seem to be localized in channels stretching down towards the metallic substrate. These pours channels may have facilitated the mass transport of nitrogen in the sample, allowing unhindered gas diffusion for the nitrogen towards the surface of the metallic substrate at 400 nm. this is also supported by the fact that there is no concentration gradient present in the N rich region region above the metallic substrate. at around 400nm the start of the metallic substrate is marked by the steady decrease in N concentration following an evolution consistent with the one observed in standard gas-diffusion nitration of Ti.

5.2.3 compositional evolution of oxygen

The Oxygen concentration is initially high towards the surface of the sample. Initially there is a 1:1 ratio of oxygen and titanium before it rapidly drops of along with the increase of nitrogen around 130 nm. It continues to decrease with a close to linear behaviour until just above the substrate interface, where a slight increase in oxygen concentration can be observed. After the it drops to bellow the observed substrate composition and stabilizes just above 10 at. % in the substrate. There is a discrepancy between the observed substrate composition and the expected composition of Ti6Al4V. The maximum value expected from the technical documentation of this Ti-alloy is 0,5 at. % this discrepancy can however be attributed to oxidation of the APT sample post preparation, as the samples where stored in air at room temperature between preparation and analysis. The high surface area and small volume makes the sample susceptible to oxidation mechanisms post preparation and it is therefore not unlikely that this is the case.

As earlier mentioned the overlap and mixing of phases does make it difficult to determine the exact composition of the phases present just from the APT analysis itself. From the XRD difractogram previously produced for the samples, shown in figure 4.1. Clear signals for rutile TiO_2 are observed, it is therefore assumed that most of the oxygen in the sample is present in the form of TiO_2. The abundance of TiO_2 quickly decreases in regions where the TiN becomes prevalent in the sample. this can be observed both in the oxide layer between 130 nm and 410 nm, and in the metallic substrate from 410 nm and down. The latter case can be an effect of the aser treatment as this is not present in the R3-2 sample as shown in figure 4.7. this can not be determined for sure as the diversity in this can be coincidental due to the fact that there is only one smaple from each texture group. this effect of an increase in oxygen, followed by an increase in nitrogen as a result of laser treatment is supported in litterature [13] This is an indication that the sample fabrication procedure of annealing the samples in a pure N_2 atmosphere. Have been effective in it purpose to limit the growth of the oxide layer.

5.2.4 Compositional evolution of vanadium

The Vanadium in the sample follows an interesting evolution. The only source of vandaium is as an alloying element in the Ti6Al4V substrate. The concentration of vanadium does however stay fairly constant at 2 at.% througout the entierty of the intermediate Oxide layer and show a drastic increase just after the N concentration decreases which coincides the region where Ba starts to appear. It is clear that vanadium readily diffuse through the entire oxide layer and possibly forming a secondary phase. Studies donne by R Böttcher *et al.* show that the solubility of V in $BaTiO_3$ is very low and that it rather forms secondary phases in the form of $Ba_3V_2O_8$ [3]. The prerequisites for the formation of such a phase is present in the sample as it forms in a region where Ba and O is present in the sample. This explanation also explain the lower Ti concentrations in this region. As the increase of vanadium that corresponds to a decrease of Ti, indicates the presence of a phase that does not contribute to the total Ti concentration. Despite this there is no indication of such a phase in the obtained XRD defractograms previously produced and shown in figure 4.1, this can however be attributed to the low abundance of the phase said phase.

The fact that vanadium is so mobile in the sample is an unexpected result in itself. Great effort was made to verify this result and investigate the possibilities for misidentifications of the elements that contribute to the total vanadium concentration. In these investigations, an exempt of the obtained mass spectra was produced, comparing 3 different regions of the sample. One from 50- 150nm, one from 250-350nm and one from 700-800 nm. The comparison between the mass-spectra from the different regions are given in figure 5.1. the figure show that ions detected as V^{2+} is more or less constant in all the three investigated region. The peak at 25,5 has approximately the same intensity in all 3 regions. The signal for ${VO_2}^+$ with a m/z of 83 show a lower relative intensity in the 250-350 nm region and is absent in the 700-800 nm region. The 25,5 peak for V^{2+} is resolvable in all regions and can with certainty be identified as vanadium, as this is a monoisotopic and single element ion there is not much room for misinterpretation. The peak assigned to ${VO_2}^+$ carries a larger degree of uncertainty, as molecular ions and ions with a higher mass opens up more possibilities for misinterpretation of the signal as another combination with the same mass. The mass spectra also show a significantly lower mass resolution in the 50-150 nm region of the sample and a significantly higher background level. This can be attributed to the high pulse energy used in combination with the very sharp tip for this particular sample. At the very apex of the sample the energy from the pulsing can not be dissipated fast enough because of the small volume of available sample in this area. As a result of this the tip retains an energy level that can facilitate a field evaporation long after the pulse has ended, resulting in a lower mass resolution. This effect will be discussed in greater detail in chapter 5.4.1

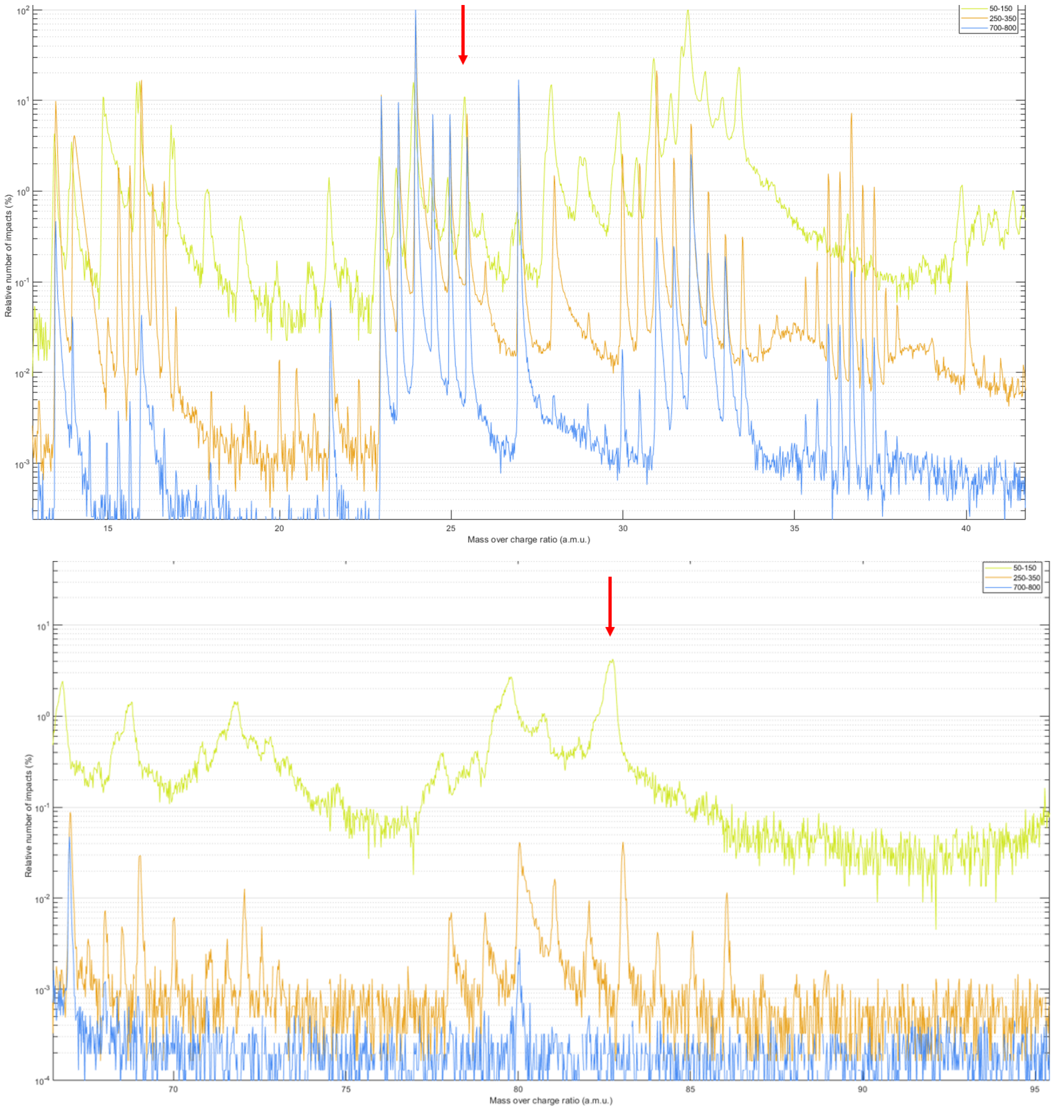

Figure 5.1: ROI mass spectra displaying the peaks at 25,5 and 83 respectively, marked with a red arrow. The green plot indicates the mass spectra in the region between 50-150nm, the orange plot annotates the mass spectra in the region between 250-350nm and the blue plot annotates the mass spectra in the 700-800nm region. The relative numbers of impact at the y-axis is in a logarithmic scale.

To be able to rule out possible misinterpretations of the peak at 83, plausible candidates was investigated by combining certain elements know to be present in the sample by the rest of the mass spectra, the closest candidate is TiO_2^+ which have a m/z of 80 with an isotopic splitting ranging from 78-82, this is however fully accounted for in the surrounding peaks and is fairly resolvable from the VO_2^+ peak even with the aforementioned loss in mass resolution. BaO^+ is expected to be found at 85 with an isotopic overlap at 83, there is however no peak at 85 and this is therefore also ruled out. Based on the lack of plausible alternatives and the conclusive evidence by the signal at 25,5 that there indeed is V present throughout entire sample. The peak at 83 can quite confidently be ranged as VO_2^+, and the results indicating a significant increase in vanadium concentration towards the top of the sample is valid and plausible.

5.2.5 Compositional evolution of Barium

Barium in is not observed in any significant amount before 200 nm, where it is observed as Ba^{2+}, slowly increasing towards the top of the sample where it is observed at a maximum concentration of 0,5 at%. This is significantly lower than expected for a $BaTiO_3$ coating. There are several plausible possibilities for this discrepancy. One likely explanation is that the APT sample is not produced sufficiently close to the surface of the material sample, and that the sample therefore only represent the region bellow the BT coating. As Ti was used as a protection layer for this sample it can not be conclusively determined that the surface of the sample was analysed as there is no clear shift in composition that indicates where the coating stops and the protection layer starts. Another factor to consider is that the analysed area of the material sample that is very small, only about 20x20 nm. It can therefore not be considered a universal representation of the entire material sample. To obtain a more statistically representative picture of the compositional evolution, data from several samples needs to be considered together.

There are as well a possibility that the analysis conditions can lead to a loss of Ba. The primary parameter to consider is the pulse frequency, this governs the detection window of the analysis. Heavier ions and clusters may be lost it the pulse frequency is set to high, as ba^{+} have an atomic mass over charge of 138, it is expected to be one of the last ions to hit the detector within the detection window. If a loss of ba^{+} due to a short detection window indeed was the case it would lead to a drastic underestimation of the ammount of Ba present in the sample. To investigate this the pulse frequency of some analyses was varied to verify that an increase of pulse frequency did not alter the obtained mass spectra. In addition, the mass spectra of bulk BT samples was briefly analysed to verify that a pulse frequency of 250 khz was sufficient to detect ba^{+}. it can therefore be determined that the absence of ba^{+} is not a result of a small detection window. This makes it likely that the Ba^{2+} is representative for the true amount of Ba in the sample, and consequently that the discrepancy indeed is because the sample is not produced sufficiently close to the surface.

5.3 Development and adjustments to the sample preparation procedure

5.3.1 Selection of ROI and parent sample

The initial experiments in the project resulted in a high amount of premature fractures, where the samples fractured in the initiation phases of the analysis not yielding any valid results that could be used for either reconstruction or concentration profile analysis in any meaning full way. The primary reason for these fractures where attributed to the highly porous samples, especially around the interface where some of the samples seemed to have voids running along the entire width of the sample as shown in sample C and certain degree B in figure **??**. This raised doubts whether or not a sufficient volume of the samples where possible to analyze with this amount of porosity. For this reason the initial samples where produced with an aim to position the apex of the APT sample as close to the porous interface line as possible, annotated as a low ROI. This was done to be able to reach and possibly cross the interface region by analysing the smallest volume of sample possible. As this porous region is the feature of the sample which marks the interface between the applied coating and the metal substrate, it was a highly interesting area throughout the project.

From the results shown in figure 4.7 of the first successful sample: R3-2, it was determined that the analysis did not provide enough data to evaluate the behavior around the interface as it did not show a stabilized coating region. The part of the sample that showed a variation in composition was also very short, as the constituents quickly stabilised to the expected bulk substrate composition. For this reason it was necessary to move the intended region of interest closer to the surface in the subsequent samples. This did increase the portion of the samples fracturing, as well as increasing the requirement for the volume of sample needed to be analysed.

By studying the different material samples provided, it was observed that the samples in texture group L showed great variation in porosity and contained some regions which showed a significantly lower degree of porosity compared to the previously used samples in texture group R, as shown in figure 3.11. for this reason the L group samples where chosen as the primary sample to analysis going forward. As they provided the possibility to achieve the highest density in the APT samples, consequently making them less susceptible for premature fractures. Samples in texture group LG and G showed an even greater degree of porosity and was therefore deemed unsuitable for APT analysis.

Sample L3-2 was prepared with a target of having a high region of interest. In order to provide data from further towards the surface compared to the initial R3-2 sample. This did provide additional information about the oxide layer further towards the surface of the sample but was still insufficient for determining the thickness of the interface region as well as determine the change in composition in this region compared to the $BaTiO_3$ coating.

5.3.2 Selection and preparation of remnant protection layers

New challenges in the sample preparation procedure did arise for preparation of the L textured samples. The variations in density of the interface layer gives rise to variations in the thickness of the coating itself. making it harder to judge where the apex of the APT sample will be placed at the end of the preparation in relation to the surface of the material sample. The surface of the L textured samples is also relatively rough as shown in figure 5.2. This has implications for the shaping of the APT needle as smaller protrusions and bumps on the surface are milled away easier than the bulk of the sample. This disturbs the natural formation of the needle shaped sample, making it asymmetrical or splitting the apex. To correct for these sub-optimal sample shapes it was necessary to mill further down in to the material sometimes up to 200-300 nm and consequently loose parts of the coating in the sample preparation process.

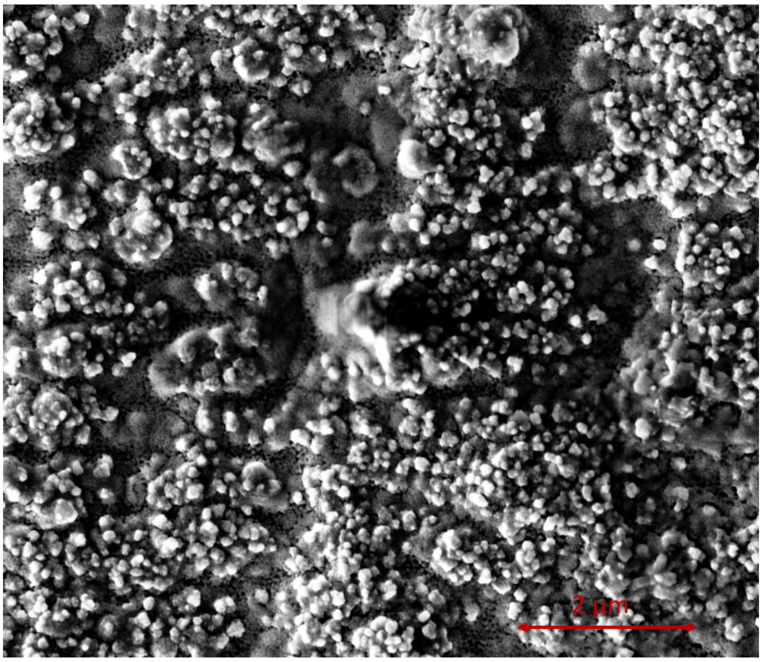

Figure 5.2: Image of the surface of texture group L

An approach was to apply an excessive amount of Pt protection layer during sample preparation, up to 800 nm. this smooths out the surface of the sample. The flat and even surface is ideal for forming a symmetrical and uniform needle during the initial shaping of the needle. The thickness of the Pt deposition was used to allow for refinement of the shape as well as shrinking the diameter of the sample without damaging and losing parts of the surface bellow. The issues with this approach was that the deposited Pt mills much faster than the Ti rich material sample. This hinders the initial and well defined apex of the sample to continue to naturally continue to the material sample during the push down and final sharpening of the needle. The shape of the apex is to a degree reset once all the Pt is milled away, resulting in large shank angles and necessitating further milling after the end of the protection layer was milled away, leading to a loss of the surface of the material sample.

To be able to prepare samples very close to the surface of the sample. it was concluded that a remnant protection layer was to be left on the finished samples. This negates the tendency that the sample shape is influenced by the transition between two materials with different sputtering yields as well as giving a larger area of valid placement of the intended ROI. The first remnant protection layer tried was simply to leave 40-80 nm of the deposited Pt protection layer on the sample. The samples prepared in this manner achieved a satisfactory shape and a total of 4 of these where attempted analysed. The samples fractured quickly when they where attempted analyzed. The issue with utilizing a material with a low evaporation-field like Pt deposited with FIB, togheter with a relative high evaportaion field like the Ti based material samples. Is that the Pt can evaporate away very quickly under fields that are not strong enough to evaporte the Ti based material sample. This stops the propagation of the apex at the transition between the Pt and material sample, leaving a flat and surface as the tip of the sample once all the Pt is evaporated away. This flat tip can not facilitate the evaporation of the high evaporation-field material at a reasonable applied field, and the sample fractures due to the high electrostatic pressure applied to the sample.

In the final iterations of prepared samples, Ti an Al protection layers where deposited using an E-beam evaporator. The protection layers where also annealed at 100 °C for 4 hours in order to give them more of a crystalline character, which is beneficial for the adhesion and evaporation-field characterstics of the protection layer. Layers deposited by E-beam evaporator also show a considerable higher purity compared to protection layers deposited by FIB, as there is no Ga impurities embedded in the protection layer as a part of the deposition method. During sample preparation these protection layers was treated as the surface of the material samples and the targeted ROI was placed to be somewhere in the lowest 100 nm of the protection layer. Efforts were made to not leave more than 40-80 nm. As that would lead to an increased analysis time and decrease the likely hood to reach the interface in the sample before an expected fracture.

The analysis of the Al protected samples where affected by the same issues that affected the previous analysed Pt samples. The predicted relative field of Al is calculated to be 19 V/nm compared to a predicted 41 V/nm for Ti[8]. Although these values are not experimental values and only apply for single element phases, they can still offer a reasonable comparison and give an indication in the relative ease of evaporation. Because of this large discrepancy in evaporation field, the Al may have been easily evaporated at a field insufficient for evaporation of the largely Ti-based material sample. And the sample the sample fractured almost instantly after all the Al was evaporated. During analysis of these samples only Al was detected with a high amount of tailing. This indicate the Al protection layer was evaporated too fast with the analysis conditions used, which can be considered a relatively high pulse energy (60 pJ) and elevated analysis temperature (50 K).

The Ti protection layer did not experience the same issues related to different evaporation fields. Since the majority of the material sample consists of Ti containing compounds it is believed that the evaporation field of the sample would be relatively close to the evaporation field of pure Ti.The Ti protected samples was therefore successfully analysed. The sample preparation procedure also benefited form using Ti as a protection layer. The major drawback of utilizing Ti as a protection layer is that it is the same element as the majority of the material sample. This makes it difficult to determine the exact start and end of the protection layer, or if it is present at all in the resulting analysis data. This is also the case for the results from sample L3-17 as there is no obvious region at the top of the sample that has a higher Ti concentration than the rest of the sample. For this reason it is difficult to conclusively determine that the surface of the material sample have been analysed. If the Ti protection layer was indeed remnant on the sample as intended, is it equally difficult to conclusively determine where it ends and how it has influenced the composition of the very top region of the sample.

The difficulty to distinguish the material sample from the protection layer was the primary reason for also utilizing a different element protection layer such as aluminium as the protection layer for the other samples. The material choice of aluminium was however unfortunate due to the described discrepancy in expected evaporation field. The initial choice of protection layer was Cr but was not available in the E-beam evaporator at the time.Al was therefore chosen as it was determined to be an intermediate between Ti and Ga infused Pt. Elements with a higher evaporation field than Ti was avoided as a too high discrepancy in this direction could lead to an evaporation of the shank rather than the apex of the sample, resulting in a micro fracture directly beneath the protection layer. This would have lead to a complete loss of the upper parts of the BT coating, greatly impacting the quality of the resulting data without necessarily being noticed during or after the analysis.

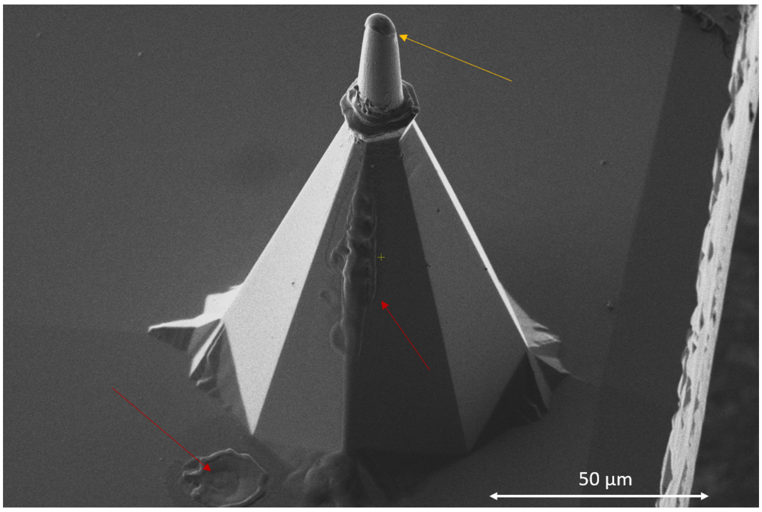

Figure 5.3: Image of the remaining sample post after a fructure, the red arrow indicates evidence that large portions of the sample post have melted, the yellow arrow indicates the top of the sample post where the sample would have been.

5.4 Discussion regarding sample fracture

A large amount of the produced samples fractured early in the analysis. A fracture occurs when the electrostatic pressure from the applied electric field becomes so high that it critically damages the sample. This is common to happen when the tip of the sample has progressed to state where the field intensification at the tip is not large enough to facilitate a field evaporation at a sufficiently low electric field. The exact mechanisms behind the fractures are not well understood and hard to examine as the sample is destroyed beyond recognition in the process and not possible to examine post fracture as shown in figure 5.3. There are however several controllable factors that impact the point of sample fracture which can be manipulated to decrease the likelihood of an early fracture. The primary way to avoid sample fracture both early and late in an analysis is to limit the strength of the field necessary to achieve field evaporation. the strength of the field necessary is largely governed by the shape of the sample. an initially very sharp tip is crucial to ensure a good initiation of the analysis at a low applied field. The shank and the shank angle of the sample is also equally important for the longevity of the sample, as this property governs how the apex of the needle will develop during the analysis. if the shank quickly becomes wider the apex will more quickly get a flat characteristic and subsequently need a larger applied field to undergo field evaporation. Some of the samples prepared did have a sub optimal shape for analysis and likely fractured because of this, such as sample B in figure **??**. As seen in the figure this sample is initially very sharp but has a high shank angle and quickly reaches a point where the shank is very wide. It also exhibits an uneven shank further limiting the possibility that the tip evolves and propagates as a sharp tip during the analysis. as the favorable point of evaporation will quickly shift from the very tip of the sample towards the edges of the triangle shaped top of the sample to the edges when their angle becomes equal, rapidly resulting in a wide tip with a round and blunt apex. The reason for these uneven tip shapes will be further discussed along with the discussion for protection layers and sample preparation.

5.4.1 Possibilites to reduce fracture rates with analysis conditions

Another way to limit the field necessary to achieve field evaporation is to increase the applied energy through increasing the pulsing energy of either the laser or HV pulses. This decreases the necessary applied electric field to achieve evaporation and subsequently the electrostatic pressure the sample experiences. However, an increase of the pulse energy may decrease the mass resolution as a high amount of energy gives a higher local heating of the sample. this increases the window in which evaporation can occur, increasing the uncertainty of the evaporation time and subsequently the TOF of the evaporated ions. For this reason, there exists an optimum pulse energy related to the material analyzed, where the pulse energy is high enough to evaporate all the components of the sample. But not so high that significant tailing and loss of mass resolution occurs. For the BT samples analyzed the mass spectra is so crowded and the pulse frequency used is already quite high compared to other similar analyses[12] that a further increase in pulse energy, and sacrificing a resolvable mass resolution for longevity of the sample would not be beneficial.

The desired detection rate also influences the necessary applied field. The detection rate governs how fast you evaporate the samples. The most common way to conduct atom probe studies are as earlier described to match the applied field to give a constant detection rate. The detection rate is determined by the average number of ions detected each applied laser pulse and a lower detection rate requires a lower applied field to achieve the desired number of detected ions. The major downside to decreasing the detection rate is the time of analysis. Fewer ions each pulse means a slower propagation of the tip and increased analysis time for the same number of ions collected. This has first and foremost practical implications, since the analysis for this application requires a large amount of ions, especially for a depth evolution of above 600 nm, which would give a continuous and complete data set for the entire coating. The longest analysis time in this project was 28 hours and yielded a depth of just above 1 um.

A lower detection rate also increases the time the sample is exposed to the electric field. It also increases the number if pulse cycles it is exposed to. This is may negatively impact the structural integrity of the sample as this may induce cyclic stresses which propagates cracks or imperfections and ultimately leading to the sample fracturing due to fatigue[15]. As the samples in this project was inherently porous with regions counting a large amount of imperfections the probability that the induced stress would intensify and propagate cracks is believed to high, relative to more common sample types with a more uniform density distribution. It is also worth mentioning that the benefits of a low detection rate are only redeemable if it prevents the sample from fracturing before it has reached a state where the tip geometry is too blunt to facilitate the evaporation under a reasonable electric field. At this point where the tip becomes too blunt the sample is expected to fracture regardless off the mitigating parameters and is largely uninfluenced by the rate of evaporation. For this reason, a reduction in detection rate not significantly increase the expected depth yield from the sample, given that the sample is otherwise structurally strong.

By reducing the expected ions evaporated by each pulse you also influence the results by increasing the noise level, as the noise arises from ionization of pollutions adsorbed to the sample or ionizations of the surfaces of the instrument itself, like the local electrode [8]. These noise events are not governed by the propagation or pulsing of the tip but can occur at random moments throughout the analysis. With a low detection rate, you expect to evaporate a low number of ions from your sample. Therefore the ratio of sample events to noise events will be lower for each pulse. For the BT samples analyzed in this project this could be influential. Both the coating layer and the substrate consists primarily of Ti, therefore the analysis and treatment of data are hugely dependent on less abundant species in the sample such as Ba and V. A higher noise level would render these species undetectable in areas of the sample and drastically reduce the quality of the results.

5.4.2 Possibilities to reduce fracture with sample manipulation

the strength and structural integrity of the sample is of major influence on the fracture point of the sample, the mitigating factors described earlier can be applied to reduce the necessary applied field, however if the sample is not structurally able to withstand the electrostatic pressure required to achieve field evaporation, the sample is not suitable for analysis with APT. The BT coating had a major porous region around the interface of the coating. This porous region which was present in the majority of the samples is a major weak point for the sample. This area is subjected to the same field intensification mechanisms which allows for field intensification at the apex of the sample, further weakening the area by evaporation of substance from this already strained area. It is also a focal point for stress intensification mechanisms where the stress induced by the pulsing laser and alternating current is amplified. In cases where the result of this stress intensification is not impactfull enough to break the sample instantaneously, is it still an area rich of cracks and defects which over the course of the analysis time can propagate and ultimately lead to a fatigue induced fracture of the sample. Despite the issues that arises from this region, it was still a highly interesting area to study, as it marks the interface between the coating and the substrate. For these reasons special considerations was made to this area during the sample preparations to attempt to limit the negative influence this area would have on the quality of the samples.

One approach was to make this area as wide as possible, to increase the amount of material available to structurally adhere the top of the sample to the bottom. Effectively this approach forfeits the possibility of being able to cross the interface during the analysis as this area of the sample is purposefully shaped to wide for a feasible analysis under reasonable conditions. This did however prove difficult to do in practice as both the coating and substrate had a relatively sputter resistant behavior and required a large amount of milling in order to make the sides of the needle even and without protrusions. that would otherwise disturb the evolution of the tip during the analysis. These protrusions formed even by lowering the increments at which the radius of the milling pattern was reduced, necessitating a longer milling time which inevitably affected the thickness of the critical porous region.

Another approach to overcome the porosity of the samples was to attempt to solder the porous region using a Pt deposition applied locally to the porous region right before the final polishing step of the sample as shown in fig xx. The reasoning behind this technique is that the Pt will act as a supporting material, that physically adheres the two regions of the sample together as well as more evenly distribute the earlier described stresses that the sample is subjected to. Another beneficial effect is that it shields the sharp edges around the porous region, decreasing the likelihood that premature evaporation of the material around this region occurs by inhibiting the field intensification mechanisms that occurs around sharp edges. The process of applying the Pt layer was unproblematic. An even and uniform Pt layer was easily deposited in a matter of seconds and subsequently polished down to match the shape of the rest of the sample, without visible pores or protrusions.

Out of the 4 samples prepared in this manner, none of them yielded a successful analysis and all samples fractured very early in the analysis. With this low amount of tried samples and a large variance in other, difficult to quantify parameters that influence the sample, like degree of porosity, degree of asymmetry, external damage etc... Makes it hard to determine of this procedure directly increased the probability of fracture or if it just did not influence the sample in any meaningful way. The first point to consider here is the type of samples this technique was tried on. All the samples showed a very localized region of porosity, with a large open area which could be easily seen and filled. It was also only applied to samples which was otherwise dense and with no apparent weaknesses other than the large, localized pores.These pores where however so substantial that the sample would likely not have survived for long during an analysis. It is Therefore a possibility that the technique was just ineffective rather than harmful to the samples.

The reasons for the ineffectiveness of the technique other than that it may not be a viable approach as there is no reported examples of this technique being successfully applied. May be linked to the combination of materials selected. Amorphous Pt deposited in the fib exhibits a lower field of evaporation compared to crystalline Ti, in general amorphous materials have a much lower field of evaporation compared to their ordered counterparts. Pt depositions from FIB is also notoriously contaminated with high amounts of Ga which have a calculated field of evaporation of 15 V/nm compared to Ti which is calculated to 41 V/nm in its pure metal form[8]. This implies that the deposited Pt is much easier to evaporate compared to the Ti based sample and it is possible that the all the deposited Pt may be evaporated before the evaporation of the Ti even starts. Rendering the applied Pt deposition ineffective in supporting the sample. Another possibility is that the deposited Pt is poorly adhered to the sample, as no annealing or measures to improve adhesion was taken. This may lead to entire chunks of the deposited Pt leaving the sample under the electrostatic pressure, potentially impacting and damage the rest of the otherwise healthy sample. This poor adhesion is difficult to address as heating and subsequent annealing the sample in its finished state can not only damage the structural integrity of the sample but may as well alter the chemical characteristics of the sample and subsequently invalidate the results of the analysis. The issue with drastically different fields of evaporation can however be addressed by utilizing different deposition materials with a field of evaporation that better matches the one of the material to be analyzed. For the case of the BT/Ti samples in this project, tungsten or carbon would likely have been a better option as they show a considerable higher field of evaporation compared to Pt. These adjustments was not tried because of a faulty module of the FIB intrument at the time.

5.4.3 Successfully applied mitigating measures against sample fracture

The only successful mitigating measure for high fracture rate, was increasing the analysis temperature from 25 K to 50 K. The primary motivation for this is to make the sample less brittle and therefore less susceptible to fatigue and inelastic deformation. But it does as well decrease the necessary field strength slightly. This is however not without drawbacks. An increase in temperature lowers the spatial resolution of the analysis. As the local energy increases induced by the laser pulsing dissipates over a larger area compared to that for when the initial thermal energy Is lower. Effectively making a larger area of the sample susceptible for evaporation events. This is most impactfull in samples with a high thermal conductivity, such as metals. Where the energy induced by the laser can be rapidly transferred to other parts of the sample, facilitating evaporation events further from the tip. This also influence the mass resolution of the sample as the flight distance in the TOF measurements gets skewed. This loss of spatial resolution is however not of major importance for the results of the samples of this project. Firstly, because ceramic samples have a lower expected resolution anyway and features bellow 4nm is not expected to be found anyway. Secondly because an atomic scale resolution is not necessary to evaluate the evolution of different species in a relatively large sample.

The other drawback which can have a major influence on the mass resolution is that the energy needed to be induced by the laser is smaller and the energy introduced to the very tip of the sample requires more time to dissipate the energy. This increases the time frame of which evaporation events are likely to occur. And the sample may in the case of the presence of materials with a low field of evaporation, emit ions the entire time frame between two pulses. This results in a massive reduction in both mass and spacial resolution[2]. For the samples coated with a Ti protection layer, this was not an issue as both the sample and the applied protection coating showed similar, high evaporation requirements. The Al protected samples did however exhibit a large amount of tailing and consequently very low mass resolution.

As no other mitigation measures where successfully applied the porosity of the produced samples was a difficult challenge to overcome. This limited the region and samples that could be analyzed to the areas of low relative low porosity at in the LIPPS textured samples. Where the high porosity to a certain degree could be avoided. The untextured reference samples, the grooved samples and the LIPPS textured grooved samples all showed a high porosity with few to no areas of low porosity. This greatly limited the scope of variation possible in the APT samples, as all samples needed to be extracted from a specific feature of the same material sample. This has likely introduced a statistic bias in the sample pool, where only a small area of similar specific sites in the material sample have been possible to analyze.

6 Conclusion and further work

6.1 Conclusion

A total of 36 APT samples where prepared as a part of this project. Out of these 20 of them where attempted analyzed with 4 of them being successfully analysed, giving information about the interface of the material sample. This low sequestrate is mainly attributed to the high degree of porosity found at the interface of the samples. To achieve a higher successes of the samples the analysis parameters was tuned to favor a decreased fracture rate rather than an increased quality of data. The samples exhibited a high field of evaporation and a high pulse energy of 60 pJ was frequently used. The Analysis temperature was increased to 50 K towards the end of the project and this resulted in fewer fractures while retaining a sufficient mass resolution. A method of soldering the porous interface layer of the APT samples to reduce fracture rates was attempted, this was however unsuccessful. Other modifications done to the sample preparation technique was utilization of different protection layers. It was found that a deposited and annealed Ti deposition made the sample preparation easier to perform and could be left on the sample without resulting in a rapid fracture of the sample. FIB deposited Pt and annealed Al was as well attempted but resulted in a rapid fracture of the sample.

One analysis yielded an exceptionally large sample volume of 1,6 billion detected ions. This yielded a sample depth of around 1,2 um and the sample displayed large parts of the produced coating layer. The large sample volume was achieved by combining the use of a Ti protection layer, a very low tip radius and an increase in the analysis temperature to 50 K. It is not conclusively determined that topmost region of the material samples where the BT coating is expected to be present, where analysed. As the amount of Ba found in the sample was only 0,5 at%. It is therefore likely that the Bt coating was not present in the prepared APT samples. This can be attributed to a very thin BT layer at the very top of the coating and the APT sample was not made close enough to the surface to include it or the APT sample was extracted from an area with a poor coverage of the BT coating. The other successfully samples was prepared much closer to the interface and did subsequently not show any Ba.

The material samples received had a differing degree of porosity and as a consequence of this the only material sample suitable for investigation was samples prepared on texture group L substrates. The other material samples showed a too large degree of continuous porosity and was deemed unsuitable for APT analysis. For this reason the effects of the laser treatment could not be investigated as both the reference sample and the most heavily textured samples was deemed unsuitable.

The analysis results clearly show a distinct substrate and a distinct coating region. The Coating region can further be separated in a region with a distinct presence of (TiN) and one which primarily consist of TiO_2 situated above the TiN containing region region. The vanadium have diffused thorough the entire sample from the substrate and accumulated at the point where Ba is present, the formation of a secondary phase consisting of $Ba_3V_2O_6$ is proposed as a possible explanation. Together these 3 regions are assumed to be the entirety of the interface layer between the BT coating and the Ti6Al4V substrate. The results can however not be regarded as a statistically accurate representation of the composition of the interface layer as only a single small volume of the material sample was analysed from a specific feature of the sample, where the porosity was low enough to be able to produce an APT sample

6.2 Continuation and further work

As the material samples have been very challenging to analyse due to their high porosity further APT investigations using the same samples will likely not be worth the effort and time needed. The high porosity of the samples not only makes it difficult to successfully analyse a sample with any significant volume, but it does awell reduce the quality of the data. it would likely not be possible to extract additional information compared to what is already presented here. This project has nevertheless shown that it is possible to analyse relatively poor samples and still get a usable result from it. This showns that there is a range of possibilities to use APT more actively in material development even for highly experimental samples which initially look to fragile for APT. Different material systems also require different experience from the user of the atom probe. This is especially true for oxides and thin films which can behave quite differently from material system to material system. By using APT for more material systems in this category it the local resources and expertise will grow and diversify, further widening the range of materials that can be comfortably and successfully analysed.

A continuation with further investigations of the material system is still interesting. As this project had major challenges with porosity in the region of interest, the analysis parameters and sample preparation was tuned to reduce the number of fractures and failed analyses. For this reason the optimal analysis parameters for the material system is still not determined with the respect to quality of data. With higher quality samples this can be done and the material system which is highly relevant for biomedical application can be more consistently analysed in the future.

To be able to determine the impact of the laser on the coating and the interface i would recommend using titanium substrates with a lower amount of alloying elements. This to reduce the amount of clutter in the mass spectra and the amount of different elements present in the sample. this eases stochiometric identification and makes reconstruction and analysis issues less likely as the variations in evaporation field occurs fewer times throughout the sample volume. An interesting approach could be to utilize the laser treatment to pre-nitrate the substrate as described by biswas et.al. [1]. As the amount of TiN in the interface turns out to be quite high this might have positive impacts on the coating adhesion. From an APT point of view it is in theory beneficial as well as the shift in field of evaporation will be smaller and less abrupt when crossing the interface. The last alteration i would suggest in order to successfully determine the effect of the laser would be to produce samples where the most intensely treated regions of the sample is easily accessible. Even though it is possible to extract an APT sample from the bottom of a groove, the amount of extra milling makes it more difficult and time consuming compared to a flat surface.

References

[1] A. Biswas, T. K. Maity, U. K. Chatterjee, I. Manna, and J. D. Majumdar. Laser Surface Nitriding of Ti-6Al-4V for Bio-implant Application. *Trends Biomater. Artif. Organs*, 20(1), Jul 2006.

[2] J. G. Brons. *Interface orientation dependent field evaporation behavior in multilayer thin films*. PhD thesis, University of Alabama Libraries, 2011.

[3] R. Böttcher, H. T. Langhammer, T. Walther, F. Syrowatka, and S. G. Ebbinghaus. Defect properties of vanadium doped barium titanate ceramics. *Materials Research Express*, 6(11):115210, oct 2019.

[4] A. Cerezo, P. H. Clifton, M. J. Galtrey, C. J. Humphreys, T. F. Kelly, D. J. Larson, S. Lozano-Perez, E. A. Marquis, R. A. Oliver, G. Sha, K. Thompson, M. Zandbergen, and R. L. Alvis. Atom probe tomography today. *Mater. Today*, 10(12):36–42, Dec 2007.

[5] Q. Chen and G. A. Thouas. Metallic implant biomaterials. *Materials Science and Engineering: R: Reports*, 87:1–57, Jan 2015.

[6] Q. Z. Chen, C. T. Wong, W. W. Lu, K. M. C. Cheung, J. C. Y. Leong, and K. D. K. Luk. Strengthening mechanisms of bone bonding to crystalline hydroxyapatite in vivo. *Biomaterials*, 25(18):4243–4254, Aug 2004.

[7] P. J. Felfer, T. Alam, S. P. Ringer, and J. M. Cairney. A reproducible method for damage-free site-specific preparation of atom probe tips from interfaces. *Microsc. Res. Tech.*, 75(4):484–491, Apr 2012.

[8] B. Gault, M. P. Moody, J. M. Cairney, and S. P. Ringer. *Atom Probe Microscopy*. Springer-Verlag, New York, NY, USA, 2012.

[9] B. Gault, M. Müller, A. La Fontaine, M. P. Moody, A. Shariq, A. Cerezo, S. P. Ringer, and G. D. W. Smith. Influence of surface migration on the spatial resolution of pulsed laser atom probe tomography. *J. Appl. Phys.*, 108(4):044904, Aug 2010.

[10] K. Hagita, T. Higuchi, and H. Jinnai. Super-resolution for asymmetric resolution of FIB-SEM 3D imaging using AI with deep learning. *Sci. Rep.*, 8(5877):1–8, Apr 2018.

[11] S.-H. Kim, A. A. El-Zoka, and B. Gault. A liquid metal encapsulation for analyzing porous nanomaterials by atom probe tomography, 2021.

[12] R. Kirchhofer, D. R. Diercks, B. P. Gorman, J. F. Ihlefeld, P. G. Kotula, C. T. Shelton, and G. L. Brennecka. Quantifying compositional homogeneity in pb(zr,ti)o3 using atom probe tomography. *Journal of the American Ceramic Society*, 97(9):2677–2697, 2014.

[13] D. Kuczyńska-Zemła, G. Sundell, M. Zemła, M. Andersson, and H. Garbacz. The distribution of O and N in the surface region of laser-patterned titanium revealed by atom probe tomography. *Appl. Surf. Sci.*, 562:150193, Oct 2021.

[14] D. J. Larson, T. J. Prosa, R. M. Ulfig, B. P. Geiser, and T. F. Kelly. *Local Electrode Atom Probe Tomography*. Springer-Verlag, New York, NY, USA, 2013.

[15] T. J. Prosa, S. Strennen, D. Olson, D. Lawrence, and D. J. Larson. A Study of Parameters Affecting Atom Probe Tomography Specimen Survivability. *Microsc. Microanal.*, 25(2):425–437, Apr 2019.

[16] M. O. H. Solum. Development of piezoelectric coatings on metal substrates for biomedical applications. Master's thesis, NTNU, 2020.

[17] G. Thornell and S. Johansson. Microprocessing at the fingertips. *J. Micromech. Microeng.*, 8(4):251–262, Dec 1998.

[18] A. A. Tseng. Recent developments in micromilling using focused ion beam technology. *J. Micromech. Microeng.*, 14(4):R15–R34, Jan 2004.

[19] X. Zhou, T. Kaub, F. Vogel, and G. B. Thompson. Complications of using thin film geometries for nanocrystalline thermal stability investigations. *J. Mater. Res.*, 35(16):2087–2097, Aug 2020.

NTNU

Norwegian University of
Science and Technology